Towards Completely Printed High-Capacity Flexible Zinc-Air Batteries

Taichong Ma

A dissertation

submitted in partial fulfillment of the requirements for the degree of

Doctor of Philosophy

University of Washington

2021

Reading Committee:

J. Devin MacKenzie

Ting Cao

Vincent C. Holmberg

Program Authorized to Offer Degree:

Department of Materials Science and Engineering

University of Washington

Abstract

Towards Completely Printed High-Capacity Flexible Zinc-Air Batteries

Taichong Ma

Chair of the Supervisory Committee:
J. Devin MacKenzie
Department of Materials Science and Engineering

Flexible thin batteries are an essential component of emerging thin, flexible and wearable electronics. In this work a completely printed thin film zinc-air battery has been demonstrated for the first time via a layer-by-layer monolithic additive process without electrolyte filling after cell fabrication. This monolithic process was enabled by the high thermal stability and low vapor pressure of the sold ionic liquid electrolyte films. These printed thin film batteries exhibited high volumetric capacities of 200 AhL^{-1} as compared to commercially-available thin film lithium polymer batteries and represents, as far as the authors are aware, the highest areal capacity(2.0mAh cm^{-2}) for any cells with thicknesses below 160 μm.[1] For batteries below 500 μm in total thickness, an aerial capacity of 2.4mAh cm^{-2} is higher than that of other flexible batteries.[2,3] The ionic liquid gel-based electrolyte is stable throughout the fabrication process which includes, cumulatively, 90 minutes of heat treatment at 80 C^{o}. Our new DES electrolyte and anode fabrication technique allow us to further reduce the overall thickness and make our battery electrolyte biodegradable. The screen printing and stencil printing tools

employed for open-air processing in this study are widely available and scalable to high production throughputs. This additive printing approach could readily be translated to large scale, low cost, and low carbon footprint production of truly thin film batteries to power next generation, low toxicity, sustainable medical devices, wearable electronics and IoT devices.

Table of Contents

Chapter 1: Overview

1.1 Wearable Electronics and Wearable Batteries

Flexible thin batteries are an essential component of emerging thin, flexible and wearable electronics as well as smart packaging, on-body medical sensing and therapeutics, and Internet of Things (IoT) wireless nodes. Although there has been a significant amount of research focused on large format batteries for applications such as electric vehicles and grid storage applications, there has been far less work on sustainable, thin and compact energy storage for ubiquitous embedded electronics, wearable electronics and the IoT. The number of small format and flexible devices in this emerging application areas, however, are forecast to reach >20B devices in 2020.[1] Therefore, it is imperative that cost effective, safe, environmentally-benign and scalably-manufactured energy storage solutions are developed to enable these devices that are expected to be present in many aspects of our day to day lives as wearable sensors[4], health monitors[5], flexible solar cells[6] and identification devices[7].

1.2 Printing Batteries on Flexible Substrates

With the advent of the Internet-of-Things (IoT) in the 21st century, there has been a pressing need to develop electrochemical devices that can be easily integrated with a wide range of surroundings for acquiring real-time data. The development of wearables has ushered in a new era of personalized IoT wherein the devices are intimately mated with the human body for various healthcare, entertainment and sports applications. Researchers have thus focused on developing wearable formats of electrochemical devices since they can play a vital role in the field of personalized IoT

Recent printing technologies that have been implemented in printed electronic devices – including electrochemical ones – can be broadly classified into template and non-template-based methodologies. Template-based printing processes can be further classified into screen printing, gravure printing, flexography, and imprinting. Screen printing involves printing inks at a low pressure using a screen mesh containing a designed pattern of uniform thickness. A metal or rubber squeegee can be used for squeezing the thixotropic fluidic ink through the patterned mesh/stencil and onto the substrate. The inks utilized in screen printing have a high viscosity but when forced through the screen mesh/stencil by the squeegee blade, they undergo sheer thinning to facilitate penetration through the screen mesh/stencil which defines the final device pattern. Upon contact with the substrate – typically a ceramic, plastic, polymeric material or paper – the ink returns to its viscous state forming the intended shape. Apart from screen printing, gravure and flexography are other genres of template-based printing technologies that are widely utilized. Gravure and flexography transfer the ink to the substrate from an engraved (gravure) or raised (flexography) patterns on a roll. This process is extremely useful for high throughput production of large-area flexible devices. For example Figure 1 is the roll-to-roll system we used to fabricate the cells discussed in this work.

Figure 1. Pilot scale advanced roll-to-roll printing system

On the other hand, non-template printing techniques comprise primarily of inkjet and 3D printing. These printing methodologies rely on localized and controlled ink dispensing onto the receiving substrate in a template-free manner. Progress in the field of engineering has resulted in complex inkjet and 3D printing processes, that involve advanced dispensing technologies involving pneumatic, piezoelectric, aerosol, electrohydrodynamic and thermal processes to print intricate, high resolution architectures. All of the above-mentioned template and non-template-based printing techniques have been extensively employed for realizing electrochemical devices, including batteries, super-capacitors, sensors and biofuel cells.

Although these printing technologies are well established, the field of wearable electrochemical devices mandates the development of a new class of printable inks with properties that enable the devices to perform flawlessly in conditions commonly experienced by the human body. For example, these printed devices must be small, thin, light, soft and should adhere well to the complex three-dimensional curvature of the

human body without causing any irritation. Such anatomically compliant printed devices should maintain conductive pathways under severe mechanical deformations and survive in a wide range of ambient conditions (e.g., temperature, humidity), and must be made of innocuous, biocompatible materials. Meeting these conditions is indeed challenging and requires innovations in materials science through the development of novel ink formulations. Significant progress in printing technology is thus required for realizing high-performance wearable electrochemical devices.

Nowadays biomedical sensors typically work at current density of 0.01mA/cm^2 [8,9]. For wireless communication a blue tooth device needs 0.2mA-0.4mA current to advertise its signal[10]. Depending on the tunning of Bluetooth devices, each advertising period is around 100ms and the rest interval is 5s-10s[10]. Since only 1-2% of the time a Bluetooth device is using it's RF unit, the average current for such device is roughly 0.04mA. Assuming the battery only need to power these two components, the capacity needs to be larger than 1.2mAh for a single day usage. And the battery needs to be able to provide at least 0.2mA for interval discharges.

Because this battery is to be attached on human body. All components should not contain hazardous materials. For comfort wearing experience the cells should have low modulus in order to match that of human skin. For maximum flexibility, the total thickness of the devices should be less than 200um since the built in stress grow linearly with the thickness.

The devices require high performance electrolyte. Since wearable devices often experience constant bending the twisting motions, the electrolyte needs to be solid state

to minimize the chance of leaking. Due to the limitation of total thickness, the cell should have minimum amount of packaging materials. Therefore, the electrolyte should have a very low vapor pressure as well. At last due to our printing process approach, the electrolyte also needs to be stable throughout the thermal processes. A typical silver or carbon ink annealing temperature is 120C^{o}.

1.3 Zinc-Air Batteries

It is proposed here that metal air chemistries are particularly attractive for high energy density thin batteries. Of the high energy density metal air chemistries, zinc air is attractive due to its low cost, ease of processing, low toxicity, and low environmental impact. Lithium-O_2 cells can access higher theoretical energy densities, however, issues related to toxicity, disposal limitations and transportation will be challenging to overcome for the use of lithium chemistries in many of the applications for thin, flexible batteries. Aluminum air chemistries can also achieve high energy densities and are more favorable than lithium-O_2 in terms of anode metal abundance, safety and disposability, however, there a limited number of non-volatile electrolytes that have been found that can effectively stabilize the Al/electrolyte interface[11].Zinc air batteries have a theoretical volumetric energy density of 6136Wh L^{-1}, which is ten times that of current lithium ion batteries and zinc is abundant, relatively inexpensive, safe for human contact and has a low environmental impact.[12]

A typical zinc air battery consists of a zinc anode, an air cathode and a basic electrolyte with concentrated potassium hydroxide (KOH). The electrochemical reaction is shown below. During discharging process, the zinc will be dissolved in the electrolyte and at cathode the oxygen from open air will be reduced.

$$Zn + 4OH^- \rightarrow Zn(OH)_4^{-2} + 2e^- \quad E^0 = -1.199V\ vs.SHE$$

$$Zn(OH)_4^{-2} \rightarrow ZnO + H_2O + 2OH^-$$

$$O_2 + 2H_2O + 4e^- \rightarrow 4OH^- \quad E^0 = 0.401V\ vs.SHE$$

$$O_2 + H_2O + 2e^- \rightarrow (HO_2)^- + OH^-\ E^0 = -0.076V\ vs.SHE$$

Zinc air batteries based on non-volatile electrolytes (NVE) are particularly attractive as they can enable additive, monolithic processing such as additive printing of solvent-based inks. NVEs allow for sequential buildup of thin, monolithic cell structures from layers that require thermal processing at each step without suffering from electrolyte loss to evaporation[13].

Metal air battery cell approaches have the potential to maintain higher capacities at lower cell thicknesses. Mechanically thinner cells experience less internal shear stresses when curved, making thinner batteries inherently more flexible. By the relationship for maximum strain versus curvature in a simple flexed sheet (Equation 1), the outer surface of that sheet experiences tensile strain and the interior surface is strained compressively.[1] Complex and asymmetric stacks, such as in a battery, can deviate from this approximation. This relationship, however, illustrates the general trend where tighter radii of curvature can be reached with reduced cell thicknesses, given finite strain failure limits for the materials and interfaces in the cell.

$$\varepsilon_{max} = \pm \frac{t}{2r}$$ *(Equation 1)*

Where ***t*** is the thickness of the sheet, and ***r*** is the radius of curvature of the bend and positive and negative signs denote tensile or compressive strains, respectively.

Metal air chemistry's inherently open to air construction and compatibility with moisture in the cell and humid ambient environments also significantly reduces the need for thick cell packaging as compared to sealed zinc alkaline or lithium-ion cells. These fundamental advantages for thin format metal air batteries enable a thin printed metal air construction and open a pathway to creating ca. 100 μm thick cells for more conformal and human contact-compatible devices in demanding applications such as

skin-adhered wireless medical sensors and ocular surface devices (e.g. ocular 'contact lens' glucosometers). As many types of closed cell batteries, such as lithium polymer, zinc alkaline or zinc carbon are scaled down to 100 microns in thicknesses, hermetic packaging and cathode thickness limitations reduce the volume available for active cell material and therefore the energy density. This, in effect, pins the minimum cell thicknesses of these approaches over 0.2mm.[14,15]

1.4 Existing Flexible Zinc-Air Battery Fabrication Methods

Typically, non-printed zinc-air batteries have been fabricated through an assembly process which includes stacking separately-prepared and cut cathode and anodes together with a mechanical separator which is later infused with a liquid electrolyte to form a complete electrochemical cell.[16–19] KOH aqueous solution (6-8M) is a common liquid electrolyte for zinc-air batteries that provides for a high ionic conductivity at low cost. Cells with high energy density (over 700Wh kg^{-1}) have been demonstrated using this electrolyte.[20,21] Incorporating polymers into the electrolyte solution to form gels can help prevent leakage and improves mechanical stability in thin cell structures.[12] Even when using gels, however, the KOH/H_2O electrolyte approach still has some drawbacks. The water in the KOH electrolyte is subject to evaporation in an open metal air cell architecture. Evaporation of electrolyte leads to a large increase in Ohmic polarization of the battery and can shorten the effective battery life.[17,22,23] Also, the high vapor pressure of water puts an upper limit on the processing temperature that the hydrogel materials can endure without significant electrolyte mass loss. Due to this limit, it can be challenging to use an H_2O-based electrolyte in a cell stack that contains sequentially-deposited layers that require post-deposition drying or curing[24]. In the same

way, the tendency for water evaporation also makes direct integration of printed H_2O-based electrolyte batteries with other electronic devices complicated.[25]

1.5 Motivation

Room temperature ionic liquids (RTIL) have been studied as ionic transport agents in lithium and zinc ion battery electrolytes due to their very low volatility and good thermal stability[26]. RTILs can also be readily formed into high ionic conductivity gels.[27] These properties makes RTIL gel electrolytes attractive for scalable cell fabrication strategies using layer by layer, monolithic printing techniques such as 3D printing, stencil printing and roll-to-roll compatible screen printing, flexography and gravure printing. Developing the processing strategy to fully print RTIL based Zinc-air battery has never been demonstrated before.

A cheaper and safer alternative of RTILs is deep eutectic solvents. The main drawbacks of RTILs are the cost and toxicity. The most common DESs contain choline chloride urea and ethylene glycol. Choline is very common supplement for poultry and agriculture[28–30] and urea is also widely available. Therefore, DESs are more suitable for large scale production and on body wearable devices due to their availability. We are not aware of any literatures demonstrating flexible zinc-air battery based on DESs. In my work I will develop the method to fabricate DES based zinc-air battery that is scalable and biodegradable.

Chapter 2: Room Temperature Ionic Liquid Based ZAB

2.1 Background

The room temperature ionic liquid is a molten salt that exists as a liquid at or below room temperature. It has a wide electrochemical window and is not easily ignited. Room Temperature Ionic Liquid has been used widely in different areas of energy storage research such as supercapacitor[31,32], zinc ion battery[33,34], lithium ion battery [35–37]and fuel cells[38,39].

Therefore, more and more attention has been paid to RTILs as substitutes for alkaline electrolytes. The inherent safety and stability of RTILs over a wide range of electrochemical potentials have led to the application of RTILs in lithium-based batteries. The use of RTILs in Zn-air batteries can effectively solve the problems of zinc electrode damage, CO_2 damage, and electrolyte evaporation in the alkaline electrolyte of the water system mentioned above and make it possible for the battery to work at high temperatures. Moreover, for aprotic RTILs, the absence of protons can effectively avoid the corrosion of the zinc electrode caused by hydrogen evolution. However the number of research publications discussing RTILs in zinc air battery is very limited at the moment.

Recently in Wei Sun's work a zinc air battery based on RTIL electrolyte is proposed. The reaction on the cathode side is 2 electron oxygen reduction reaction.[40] In the work they demonstrate that, although the 2 electron ORR results in a lower working potential, the cells showed better cycling stability compared with alkaline electrolyte cells. The electrolyte used in the cell is Zinc trifluoromethanesulfonate(Zn(OTf)). Therefore, It also

benefits from having RTILs in general such as good thermal stability, no CO_2 poisoning and no dendrite formation.

RTILs used as an electrolyte for Zn–air cells, zinc oxidation to Zn^{2+} during discharge, and the reversible electrochemical reaction of zinc in RTILs has proven to be feasible. One issue should be noted here is that incorporating RTILs may form insoluble substances with Zn^{2+} and make them unable to be reduced effectively. The mechanism of air electrode in RTIL electrolyte was proposed.

When oxygen reduction occurs in the RTIL electrolyte, oxygen gains electrons and forms a peroxide. This reaction is considered quasi-reversible. For aprotic RTILs, there is no further electron transfer due to the presence of superoxide. In contrast, for protic RTILs, superoxides are strong nucleophile that can further react with protons in RTILs to form per-hydroxy radicals. Then, per-hydroxy radicals can also react with superoxides to form peroxides and finally complete the reduction process.

2.2 Device Architecture

The target device structure is illustrated as figure 2. The purpose of this design is to

Figure 2. Cell Structure

The Cell consists of four main components. At the bottom there is the silver current collector. The second layer is zinc particle based anode layer. Third layer is the RTIL gel layer. The function of this layer is to transport ions to facilitate the electrochemical reaction and stop cathode from contacting the anode physically. Finally the cathode is coated directly on top of the electrolyte gel layer followed by a final annealing process. Annealing processes are essential to drive all solvents away from the cathode to allow air access to the cathode pores. Therefore, all the layers printed prior to the cathode layer have to be stable at elevated temperature(over 80^{o}C) for at least 40min. This is the reason why ionic liquid is an crucial part of the device due to it's good thermal stability and ultralow vapor pressure.

2.3 Fabrication Method

Bottom Current Collector Preparation

Silver paste (AG-510, Applied Ink Solutions) was printed on Kapton Tape (30 μm in thickness) by an automated 3D printer (nScrypt). After drying on the heated printer bed at 120 Celsius for 20 minutes the conductive silver 1cm*3cm*10 μm electrodes are obtained.

Flexible Zinc Electrode Preparation: 0.8g of poly (vinylidene fluoride-co-hexafluoropropylene) (Arkema Kynar Flex) was first dissolved in 8ml of 1-Methyl-2-pyrrolidinone (Alfa Aesar) to produce a binder solution. 9g of Zinc powder, 0.2g of conductive carbon black (TIMCAL Super P) and the prepared binder solution were added to a 250ml mixing jar. The mixing jar was then moved to a planetary centrifugal vacuum mixer (ARV-310 THINKY MIXER). Mixing was conducted at at 1800 rpm for 15 minutes under 0.5atm pressure to form a printable zinc electrode paste. The obtained zinc paste was then 3D printed on top of the silver current collector. The sample was dried for 20 minutes at 80 Celsius. The final film thickness of the printed Zn composite electrode was 40 μm.

Solid Electrolyte: 3g of PVA (Polyvinyl Alcohol M.W 146,000~186,000, 99% hydrolyzed, Sigma Aldrich) was dissolved in 30ml DI water at 85 Celsius. 6ml of 1-Butyl-3-methylimidazolium hydroxide ([bmIm]OH) solution (20%wt in ethanol, AngeneChemical) was slowly added to the polymer solution and the resulting mixture was stirred for 3 hours. After cooling down to room temperature, the mixed, viscous solution was 3D printed on to the zinc electrode and cured at 60 Celsius for 30 minutes. The resulting solid ionic polymer gel films were 30-50 μm in thickness.

Catalyst/Carbon Nanotube Cathode and Silver Current Collector: The synthesis protocol for the $MnCo_2O4$ / nitrogen-doped reduced graphene oxide (rGO) catalyst carried out here was adapted from previously-published work.[41] 2-4 layer graphene oxide (Cheap Tubes Inc.) was used as the rGO precursor. In a typical synthesis 9mg of GO was dispersed in 30ml of ethanol and mixed with 0.5ml Co(OAc)2 solution(0.6M), 0.25ml Mn(OAc)2 solutioin(0.6M), 0.3ml of DI water and 0.5ml of NH_4OH at RT. The solution was stirred at 80^{o}C for 12h and transferred to an autoclave. After that the mixture was heated to 150^{o}C for 3h. The resulting $MnCo_2O_4$ decorated N-rGO catalyst solution was washed with ethanol and water then freeze dried to produce a dry powder. Then, 30 mg of the catalyst powder was redispersed in 10ml of ethylene glycol (Sigma Aldrich). 300mg of aligned carbon nanotubes(nanostructured & amorphous materials Inc.) were sheared in a high shear blade mixer to obtain fluffy, low density carbon nanotube material.[42] The low density CNT material was then mixed with the catalyst/EG dispersion using a vortex mixer. The mixture was then stencil printed on top of the electrolyte layer and dried in an oven at 80 Celsius for 40 minutes to produce a 30 μm thick catalyst/conductive cathode layer.

A silver current collector was then 3D printed on the cathode using the AG-510 (Applied Ink Solutions) silver paste to minimize series resistance losses. The completed battery is then dried in an ambient pressure convection oven at 80 Celsius for 20 minutes to cure the current collector.

2.4 Characterization and Results

Physical Characterization: A Scanning Electron Microscope(SEM) (FEI Sirion XL30 and Phenom ProX), A Transmission Electron Microscope(TEM) (FEI Tecnai G2 F20) and a laser confocal microscope (Olympus OLS41) were used to characterize the morphology of the electrode materials and the electrolyte. Thermogravimetric analysis (TGA) (Mettler Toledo) was used to test the thermal stability of the electrolytes. The temperature ramping speed for the TGA tests was 10K min^{-1}

Electrochemical Characterization: Electrochemical impedance spectroscopy (EIS) (Versastat) spectra were taken for the cells at the cell open circuit voltage. The EIS perturbation voltage amplitude was 10mV and the frequency range for the EIS spectra was from 100kHz to 0.1Hz. The ionic conductivity of the electrolyte layer was measured in common electrode cells with a 100mV EIS perturbation and a frequency range from 100kHz to 0.1Hz. The voltage and discharge tests were conducted at constant current density with a cutoff voltage of 0.5V using Keithley 2450 and Maccor 4000 Series test equipment. The working potential was determined by averaging the operating potential after discharge of a cell at a fixed areal current density for 600s.

Result and Discussion: In this work, we have demonstrated a novel fabrication approach for completely printed thin film zinc-air batteries based on ionic liquid-based solid-state electrolytes. This is the first time that a completely additive process for metal air batteries, including printed anodes, electrolytes, catalysts and current collectors, has been demonstrated, opening a new manufacturing approach for thin energy storage based on low toxicity, abundant materials. This approach reduces the number of process steps and streamlines the process flow by continuous direct printing and

thermal processing. In addition, this process also allows for integration of batteries with other components that require additional thermal processing and allows for the embedding of batteries within 3D printed structures based on typical thermoplastic resins. The cells in this work were fabricated in a monolithic, layer-by-layer sequence without a later infusion of liquid electrolyte. The printed ionic liquid based electrolyte gel used here not only facilitates the ion transport but is also physically stable enough to mechanically and electrically separate the electrodes during an additive, layer by layer printing process with thermal drying steps for subsequent layers. The as-prepared, ~140 μm thick batteries had areal capacities of (2.0 mAh cm^{-2}) and volumetric capacities of 143 mAh cm^{-3} at current densities of 6.67 mA cm^{-3} at 0.8V discharge potential.

As far as we are aware, the cells produced here represent the thinnest printed batteries produced to date. This thin, printable battery overcomes the challenges associated with aqueous or volatile solvent-based electrolyte evaporation. The efficient fabrication method enables scalable large-scale production by low cost, additive roll to roll and sheet printing. Furthermore, the battery chemistry is based on low toxicity and low environmental impact materials in a robust thin format without free or volatile liquid, making it ideal for applications such as disposable medical devices, supply chain asset tracking and monitoring labels, and IoT devices.

The structure of the novel printed Zn air polymer RTIL battery is illustrated by Figure 3. The total thicknesses of the devices ranged from 140-160 μm. The fabrication sequence began with the 3d printing of a patterned current collector layer (Layer 1) using a silver particle/polymer binder ink on a polyimide substrate to provide an efficient electrical bottom contact. The zinc electrode (Layer 2), 1-n-butyl-3-methylimidazolium hydroxide

([bmIm]OH)/ poly (vinyl alcohol) (PVA) gel(Layer3), catalytic air cathode(Layer 4) and top silver contact(Layer 5) were subsequently printed, with interleaved drying steps, in a monolithic, additive sequence (details are provided in the Experimental Section). The anode, as shown in Figure 3, consists of zinc alloy particles, conductive carbon black additive and a poly(vinylidenefluoride-co-hexafluoropropylene) (PVDF-HFP) polymer binder. The zinc particles are alloyed with Bi and In to suppress the hydrogen evolution reaction during further annealing steps[43]. The relaltively large zinc particle size, >25 μm, reduces the surface area and therefore parasitic oxidation reaction rates during processing. More detail review on anode stability has been done[12] by previous study. Carbon black was added to the Zn ink to improve the electrical conductivity of the anode. The PVDF-HFP anode binder provides for sufficient flexibility of the composite electrode film and enhances the bonding of Zn particles and carbon black and prevents dissolution of the binder and disintegration of the anode during the printing of overlying cell layers in subsequent processing steps. The overlying electrolyte layers utilize orthogonal solvents to the PVDF-HFP. The viscosity of the anode ink was optimized for printing by tuning the mass loading of solvent (N-Methyl-2-pyrrolidone(NMP)) in the ink formulation.

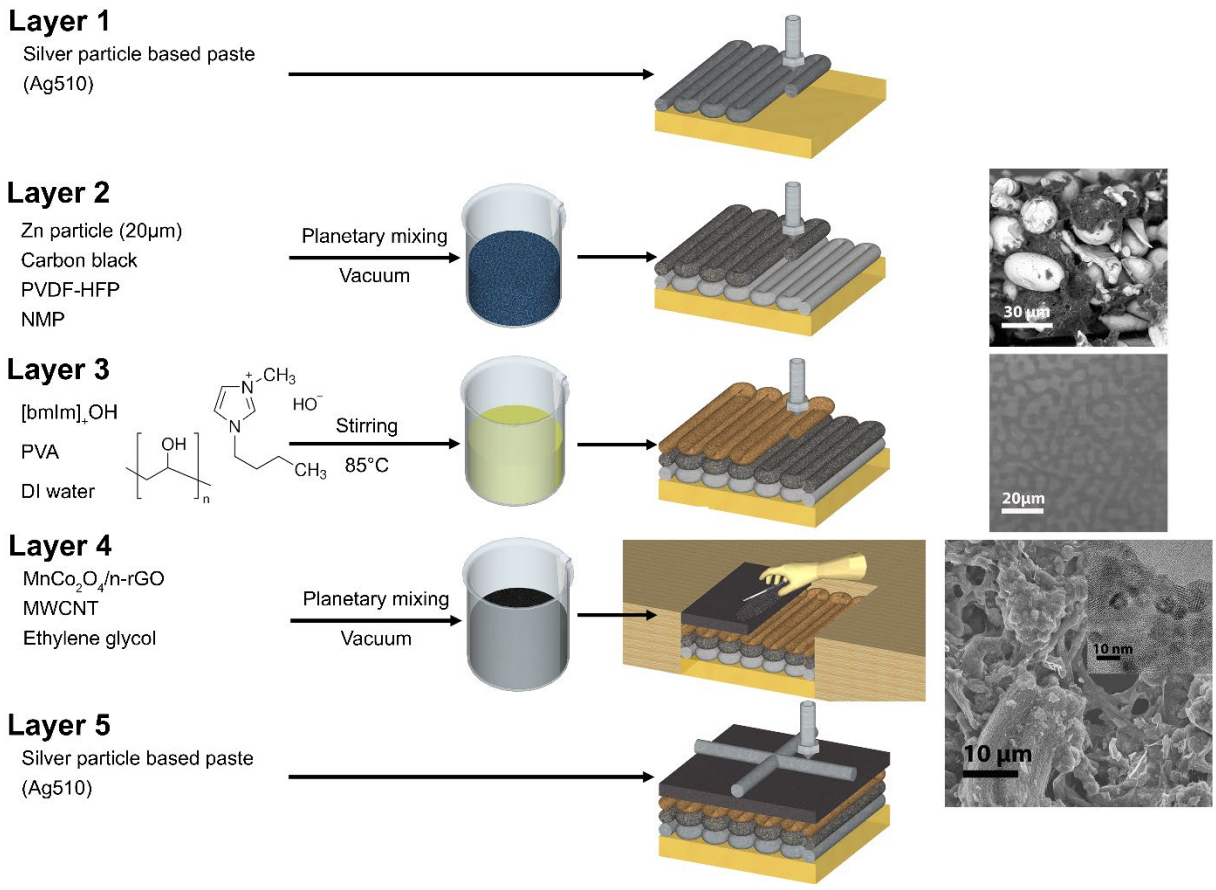

Figure 3. A schematic illustration of the battery ink preparation and layer-by-layer printing process with microscopy images of the printed materials.

The printable [bmIm]OH/PVA gel electrolyte ink was a direct mixture of [bmIm]OH and PVA water solution. After this electrolyte ink is 3D printed to form a film and thermally-treated, a phase-separated structure was observed using laser confocal microscopy (Olympus LEXT OLS4100) with micron-scale continuous domains of [bmIm]OH rich phase (Figure 3c and Figure 3f). The [bmIm]OH directly facilitates hydroxide ion transport. The ionic conductivity of the 10% IL electrolyte film shown in Figure 3f was 1.1 mS-cm^{-1}, consistent with prior studies.[44] These lower [bmIm]OH/PVA ratio

electrolyte films did not exhibit the visibly continuous structures that were observed in the 50wt% [bmIm]/PVA electrolyte (Figure 4c). The hierarchical oxygen reduction reaction catalyst (Figure 3. Layer 4 inset) and current collector is nanoscale $MnCo_2O_4$-decorated, nitrogen-doped reduced graphene oxide ($MnCo_2O_4$/N-rGO). The direct coupling of the high interfacial area $MnCo_2O_4$ particles and N-rGO provides for strong ORR catalytic activity.[41] The as-prepared catalyst was mixed with multiwall carbon nanotubes to form a permeable air catalyst electrode. After annealing, the conductive nanotubes formed a micro- and nano-porous hierarchical structure with a high surface area coverage of $MnCo_2O_4$/N-rGO catalyst (Figure 3 Layer 4), providing efficient homogenous oxygen delivery to the reaction site.

As shown in Figure 4a, the battery with 50wt% ionic liquid concentration delivered almost twice the capacity of the lower ionic liquid concentration battery and exhibited a higher working voltage at 0.1mA cm^{-2}. To evaluate the specific capacity of the battery, the battery was discharged at discharge rates ranging from 0.0375mA cm^{-2} to 0.2mA cm^{-2} (Figure 4b). A high volumetric specific capacity of 142.8 Ah L^{-1} was achieved at 0.1 mA cm^{-2}(7.14 A L^{-1}) as shown. The specific capacity is calculated to be 298.5mAh/g_{zn} which is comparable with large format zinc air batteries[19,23,45]. The capacity of the battery is much higher than other printed flexible batteries like Zn-MnO_2 [46]and zinc silver oxide batteries[47]. The smaller measured capacities at lower current densities is attributed to competing anode side reactions. The Nyquist plot of the battery (Figure 4c and Figure 4d) measured before the discharge test shows that our battery has a series resistance (R_s) of 20.1 Ω, an interfacial resistance(R_{int}) of 16.7 Ω and a charge transfer resistance(R_{ct}) of 1250 Ω. The Nyquist plot has a significant Warburg impedance

component that indicates that the catalyst is flooded with electrolyte. This is consistent with our open circuit voltage data (1.1V) which is lower than the open circuit voltage of batteries following the standard $2Zn + O_2 \rightarrow 2ZnO$ reaction (E_o + 1.59V) that practically reaches 1.4-1.5V with enough oxygen supply.

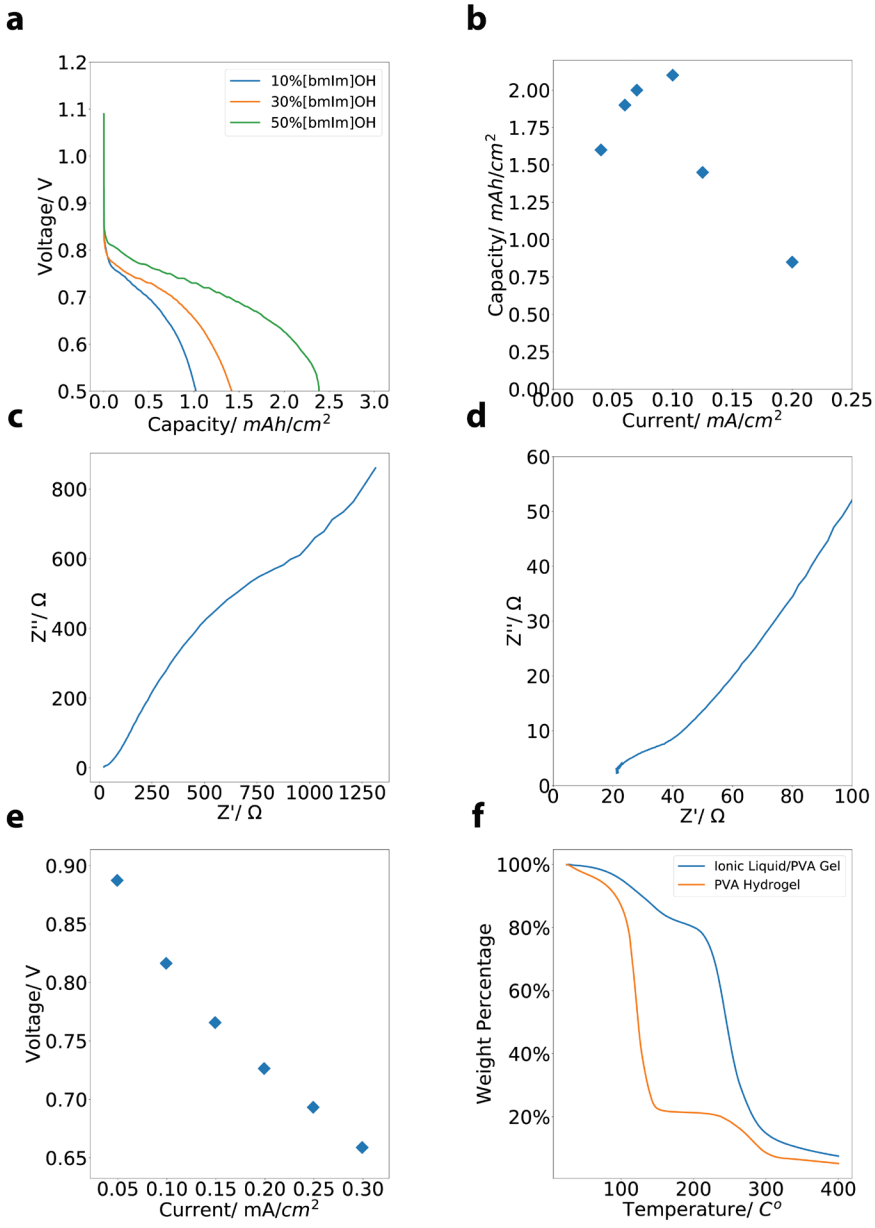

Figure 4. (a) Discharge curve of the printed cells at 0.1mA/cm^2 with ionic liquid concentrations ranging from 10wt% to 50%. (b) Capacity of batteries at various discharging currents. (c) Nyquist plot of the cell at open circuit voltage. (d) High frequency region of the Nyquist plot. (e) 10min average working potential at various discharge currents. (f) TGA data of the Ionic liquid based electrolyte and PVA gel.

As shown in Figure 4e the working potential enters a linear regime when current is larger than 0.1mA cm^{-2}. Based on the thermal gravimetric analysis(TGA) data (figure 4f) the ionic liquid based electrolyte shows superior thermal stability. The organic electrolyte undergoes full decomposition at 250C^{o} while the aqueous gel electrolyte loses water rapidly at temperature above 100C^{o}. The ionic liquid electrolyte contains around 20wt% water at 24% relative humidity (RH) and the water loses slower than the PVA gel samples as shown in the TGA data. Water participates in the ORR reaction as a proton donor which facilitates the 4-electron reaction path. Without water or other proton sources the ORR will be on the 2-electron peroxide route which is slower and reduces the energy density [48,49]. Zinc air batteries with ionic liquid electrolyte is still a relative new area of study. Because most of the well-studied ORR catalysts do not work well with ionic liquids[49], the power density (or c-rate) from this type of battery is typically limited. Compared with zinc air batteries made from other protic ionic liquids,[50] however, the battery developed here has much higher power density.

The 50wt% IL in PVA electrolyte sample demonstrated superior ionic conductivity of 9.5mS cm^{-1} as compared with other formulations (Figure 5a). This 50% IL formulation contributes to higher operating cell voltages as shown in Figure 5a. The reason is that the higher IL concentration caused significantly higher conductivity of electrolyte. High IL loading also lower the viscosity of the electrolyte which improves the infiltration of electrolyte into the anode. The average areal Zn mass density in the cells was 6.7mg cm^{-2}. Based on this density and an assumption of 2 electrons discharged per Zn ion, we calculate an anode utilization of 29.9% in the 50wt% IL cell. The surface morphology of

the Zn/electrolyte interface of discharged and as-prepared cells, as imaged by scanning electron microscopy, are dramatically different (Figure 5c-d). Compared with the undischarged anode particle shape in Figure 3b, the discharge product particles in Figure 5c form an apparently continuous film (~10 μm in thickness,) that covered the surface of the Zn particles at the anode interface and can also explain the decrease in the battery operating voltage. In the as-prepared anode/electrolyte interface in Figure 5d, there are also nano-scale particles between the zinc particles which indicates some corrosion of the Zn electrode during the fabrication process which was conducted in open air. In all cells, the discharge product was also distributed into the electrolyte and formed isolated nanoscale particles instead of passivating the Zn electrode surface. The brighter backscatter from the particles in the anode and above the anode/electrolyte interface in the SEM image in Figure 5b shows how zinc is distributed through the cross section of the discharged cell. In this case, the presence of Zn-containing precipitates more than 10 μm into the electrolyte film suggests that the IL electrolyte performs a discharge product storage function in addition to its electrode separation and ion transport role.

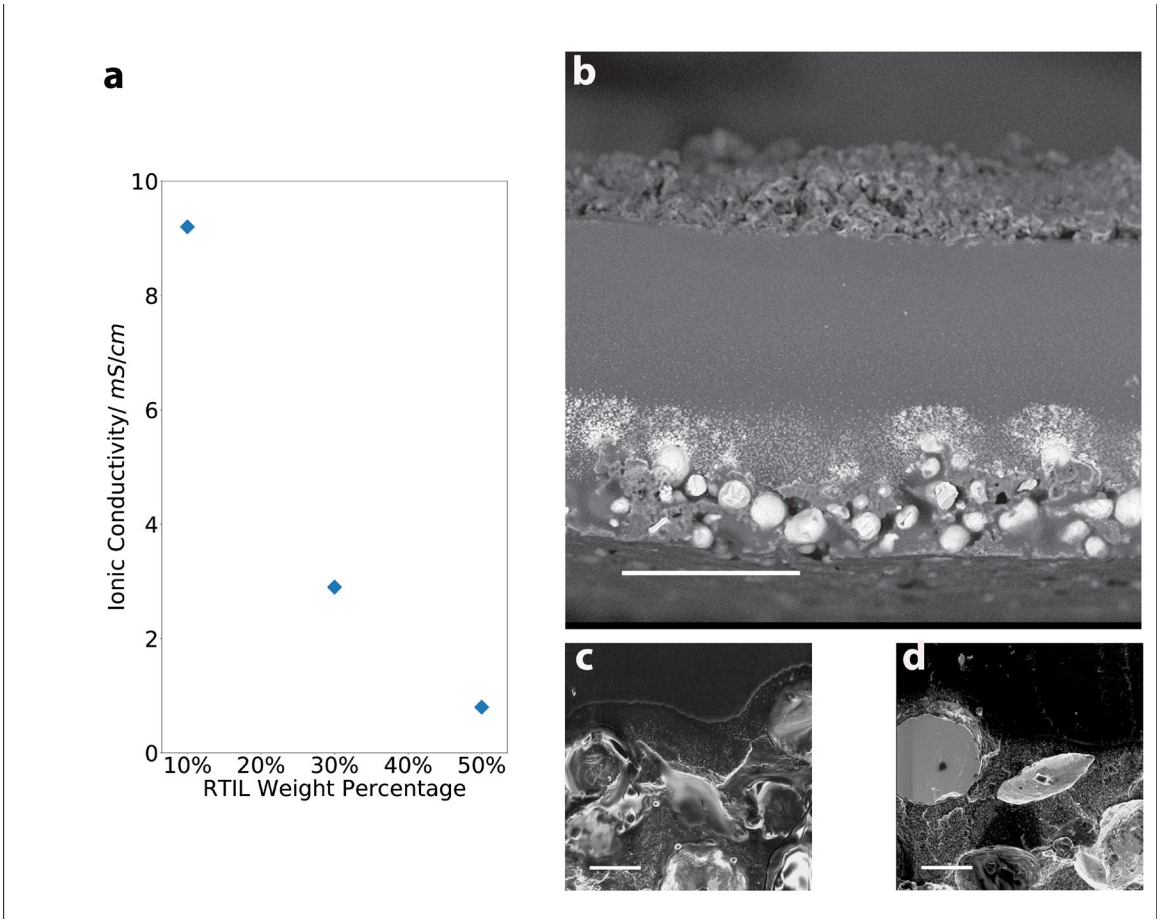

Figure 5. (a) Ionic conductivity of electrolyte films with ionic liquid concentrations ranging from 10wt% to 50wt%. (b) Cross section SEM image of a discharged battery with 50wt% ionic liquid electrolyte. Scale bar is 100 μm (c) Cross section SEM image of a fully discharged anode/electrolyte interface. Scale bar is 10 μm (d) Cross section SEM image of an as fabricated anode/electrolyte interface. Scale bar is 10μm

2.5 Summary

In summary, a completely printed thin film zinc-air battery has been demonstrated for the first time via a layer-by-layer monolithic additive process without electrolyte filling after cell fabrication. This monolithic process was enabled by the high thermal stability and low vapor pressure of the solid ionic liquid electrolyte films. These printed thin film batteries exhibited high volumetric capacities of 200 AhL^{-1} as compared to commercially-available thin film lithium polymer batteries and represents, as far as the authors are aware, the highest areal capacity(2.0mAh cm^{-2}) for any cells with thicknesses below 160 μm.[1] For batteries below 500 μm in total thickness, an areal capacity of 2.4mAh cm^{-2} is higher than that of other flexible batteries.[2,3] The ionic liquid gel-based electrolyte is stable throughout the fabrication process which includes, cumulatively, 90 minutes of heat treatment at 80 C^{o}.

We also successfully demonstrated heirarchical nanocatalyst structure based on reduced graphene oxide using hydrothermal method.

Chapter 3: Deep Eutectic Solvent Based ZAB

3.1 Background

The selection of electrolyte is vital because it can affect the performance of a battery. There has been a great deal of interest in deep eutectic solvents(DESs) from battery scientists because of advantageous properties in common with ionic liquids. Compared with conventional aqueous electrolyte, DES-based electrolytes contain the following advantages: a wide electrochemical window, ease in preparation, low vapor pressure and low cost. In contrast to many ionic liquids, DESs are biodegradable, non-toxic, and several times cheaper than ionic liquids. By now, DESs have been applied to several electrochemical systems. Normally, DES is composed by an organic halide salt with another material possessing the capability of forming a complex with the halide. For example, choline chloride and urea with the mole ratio of 1:2. This mixture is one of the most promising DES systems owning to its large metal-salts solubility. choline is a dietary nutrient and choline and urea are biologically derived and produced in large industrial quantities in agricultures. Apart from above components, additives also play an important role in gel polymer solid state electrolyte. On the one hand, in order to improve the concentration of conductive ions within a battery, some anode metal oxides need to be added into the gel electrolyte system. On the other hand, for the purpose of satisfying the requirements of printing, the gel polymer electrolyte solution should have a high viscosity. Only under such circumstance can we acquire a desired electrolyte pattern owing to a viscous fluid moves a little bit or not after printing process. We are also trying to form a gel with a yield stress or thixotropy such that it holds its shape under low shear stresses but flows when pushed at higher shear rates such as those

that occur in screen printing and nozzle-based printing. For instance, silica is a good additive for enhancing fluid's viscosity.

3.2 Motivation and Device Design

In the previous work presented in this dissertation, an RTIL was used as a physically and thermally stable electrolyte for printed ZAB. Together with PVA the gel electrolyte also acts as a separator. Because of the high thermal stability and low vapor pressure of the RTIL, the printing each layer on top of the previous one is demonstrated possible. Despite the fact that the process is scalable, the imidazolium based ionic liquid is very expensive and hard to preserve. Since the target application of this type of battery is to power wearable devices, materials with few human hazards are highly needed to fabricate the battery.

The new DES battery will follow a simple monolithic structure similar to the structure used for the RTIL gel ZABs. The anode is at the bottom of the cell and cathode at the top to maximize free air exposure to catalyst. Glutaraldehyde is used to crosslink the PVA to further enhance the 3d structure of the solid-state electrolyte. This method was not possible in the alkaline RTIL project due to the strong reactivity of glutaraldehyde with OH^-.

3.3 Fabrication Method

Fully additive flexible Zn electrode preparation based on roll to roll printing: First the current collector was flexographically printed from a nanoparticle Ag ink using an FOM X-3 roll to roll system with in line drying. One example of the silver pattern is shown in Figure 14. The patterns on each band are connected by silver bus wires. The resulted silver pattern is then submerged in electroplating bath and plated at 12mA/cm^2 for 15min.The electroplating was done at room temperature, 99.99% purity Zinc foil was used as the counter electrolyte. The electrolyte bath contains 1M of ZnSO4 and 0.1M of H3BO3. The sample is then rinsed with copious amount of DI water. It is then dried for 20 minutes at 80 Celsius. The final film thickness of the printed Zn composite electrode was 12 μm.

Thermal Cured Solid Electrolyte: 3g of PVA (Polyvinyl Alcohol M.W 146,000~186,000, 99% hydrolyzed, Sigma Aldrich) was dissolved in 30ml DI water at 85 Celsius. Urea and choline chloride are mixed at molar ration 2:1 at 80C^o. 1g of the DES mixture and 5g of the PVA solution was them homogenized in a planetary mixture at 1800rpm for 15min. Glutaraldehyde 3% (w/w) is the added to the mixture. The resulted DES/polymer ink was then coated on top of the zinc layer. The solid ionic polymer gel films were 20-30 μm in thickness.

Catalyst/Carbon Nanotube Cathode and Silver Current Collector: The synthesis protocol for the $MnCo_2O4$ / nitrogen-doped reduced graphene oxide (rGO) catalyst carried out here was adapted from previously-published work.[41] 2-4 layer graphene oxide (Cheap

Tubes Inc.) was used as the rGO precursor. In a typical synthesis 9mg of GO was dispersed in 30ml of ethanol and mixed with 0.5ml Co(OAc)2 solution(0.6M), 0.25ml Mn(OAc)2 solutioin(0.6M), 0.3ml of DI water and 0.5ml of NH_4OH at RT. The solution was stirred at 80^oC for 12h and transferred to an autoclave. After that the mixture was heated to 150^oC for 3h. The resulting $MnCo_2O_4$ decorated N-rGO catalyst solution was washed with ethanol and water then freeze dried to produce a dry powder. Then, 30 mg of the catalyst powder was redispersed in 10ml of ethylene glycol (Sigma Aldrich). 300mg of aligned carbon nanotubes(nanostructured & amorphous materials Inc.) were sheared in a high shear blade mixer to obtain fluffy, low density carbon nanotube material.[42] The low density CNT material was then mixed with the catalyst/EG dispersion using a vortex mixer. The mixture was then stencil printed on top of the electrolyte layer and dried in an oven at 80 Celsius for 40 minutes to produce a 30 μm thick catalyst/conductive cathode layer.

A silver current collector was then 3D printed on the cathode using the AG-510 (Applied Ink Solutions) silver paste to minimize series resistance losses. A metal needle with 120um opening diameter was used as the nozzle. The back pressure was kept at 7psi for consistent ink flow. The printing speed was 20mm/s. The completed battery is then dried in an ambient pressure convection oven at 80 Celsius for 20 minutes to cure the current collector

3.4 Characterization and Results

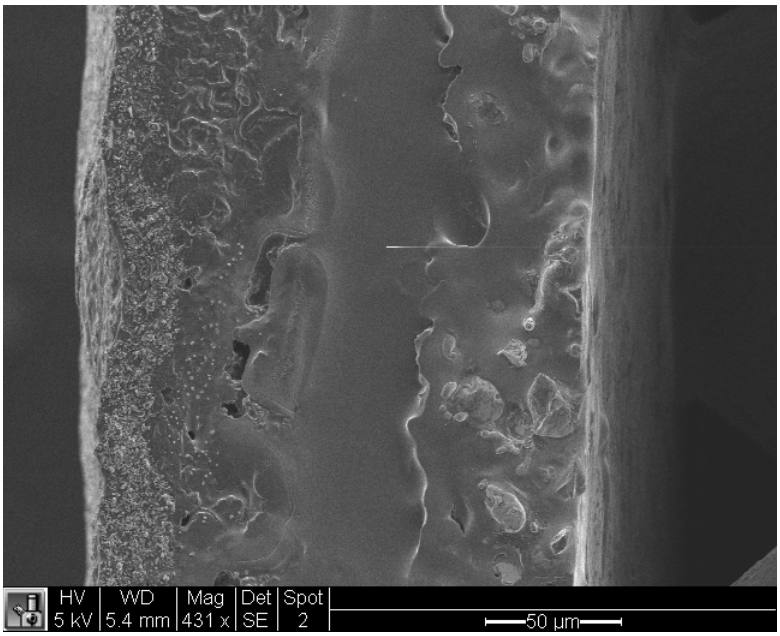

Figure 6 Cross sectional image of discharged battery

The overall structure of the des based batteries is the same as the RTIL based devices as shown in Figure 6. The components from left to right are cathode, electrolyte, anode and silver current collector. The sample was previously treated with liquid nitrogen and cross section was created by cryo-cracking method. The bottom silver layer was printed by the flexographic print head on a roll-to-roll system or 3D printing method. This method demonstrates the scalability of this fabrication process and reduces the thickness of bottom silver layer from 5µm to 200nm. It allows us to reduce the thickness of electrolyte to 20µm without forming electrolyte defects which causes internal shorting of the devices. Figure 7 shows the plane view of screen-printed zinc electrode and how it's deposited using 3D printing method(right). Our current device thickness is 170µm including the substrate(30µm).

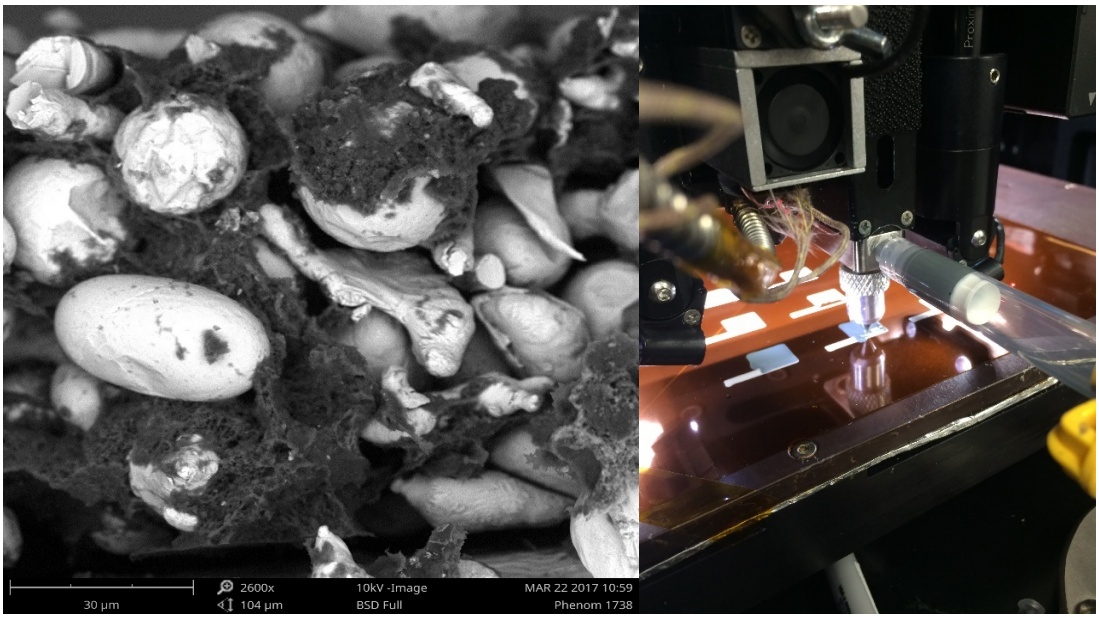

Figure 7. Plane view of Screen printed zinc electrode and 3D printing Zinc directly on Silver

As shown in figure 8, the battery has capacity over 2.4mAh/cm^2. The volumetric specific capacity is 240mAh/cm^3. The superior capacity originates from the thickness of the battery. The unstable working potential indicates electrode mechanical failure.

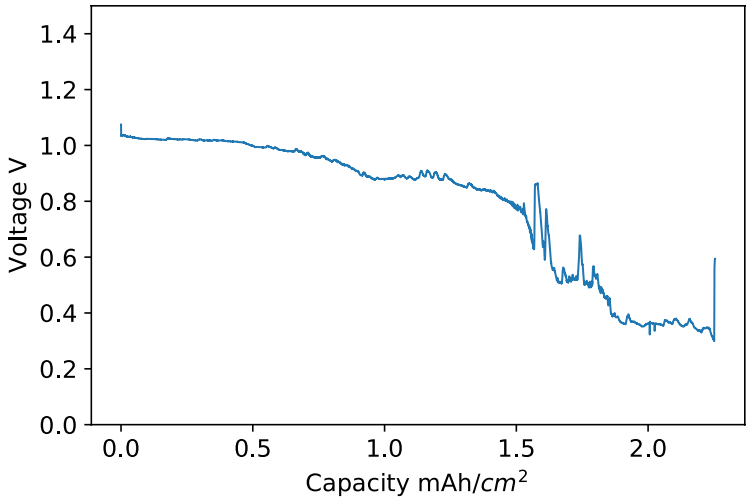

Figure 8. Primary discharge curve of DES based battery.

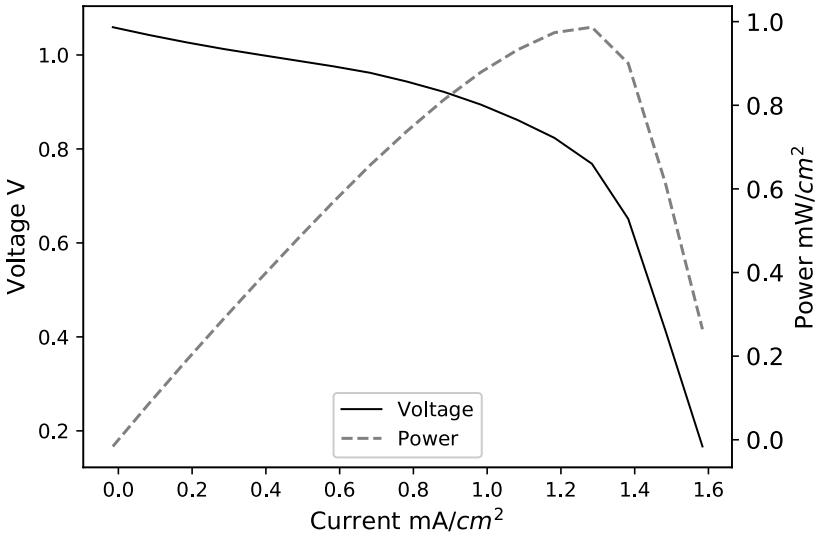

Figure 9. Galvano dynamic measurement of DES based battery

As shown in Figure 9 the battery shows a high peak power density as 0.98mW/cm^2 or 98mW/cm^3. To simulate the usage condition of a blue tooth device the battery is tested with high current discharging pulses and long resting time. Figure 12 shows the

discharge working potential of a battery tested with 5mS discharging pulses. Each pulse is 5mA/cm and the battery rest for 10s after each pulse.

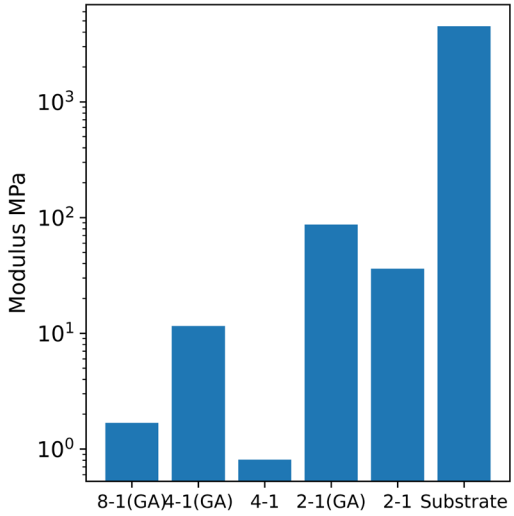

Figure 10. Young's Modulus of samples

The Young's modulus of the electrolyte gels is measure using the nanoindentor(TI 980 TriboIndenter) Each sample was measure at 16 different spot and a median value is taken. A diamond conical tip is used for this measurement. The nominal radius is 4-6μm and the cone angle is 60°. The sample names are the mass ratio between DES and PVA and whether it has been crosslinked by GA or not.

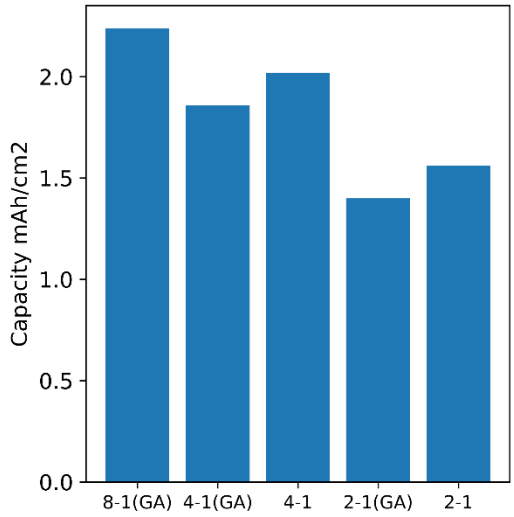

Figure 11. Primary discharge capacity vs formulation

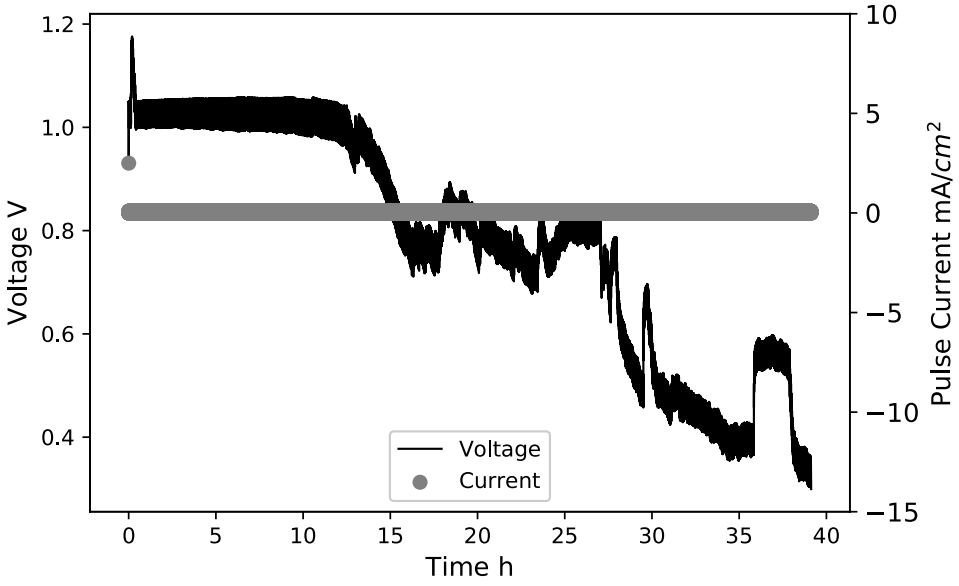

Figure 12. Pulse discharge curve (5mS pulse, I=5mA/cm^2)

Figure 13 shows the battery is rechargeable and can operate for more than 20 hours. The capacity that the battery can be cycled during discharging process is 1.22mAh/cm^2 on average. This is 51% of the maximum capacity of the cell with single discharge measurements. The discharge stops at 0.6V which is the cut off voltage. An depletion region appears at the end of each cycle which indicates a near 100% depth of discharge during cycling. It is observed that the battery is rechargeable if the electrolyte layer is chemically cross linked. 1%(w/w) glutaraldehyde is added in the electrolyte to crosslink PVA chemically. Without crosslinking, we have no data showing successful recharging cycles even when the cell is able to undergo normal primary discharge tests. Therefore the extra stability of the electrolyte contributes to the cyclability of the cells.

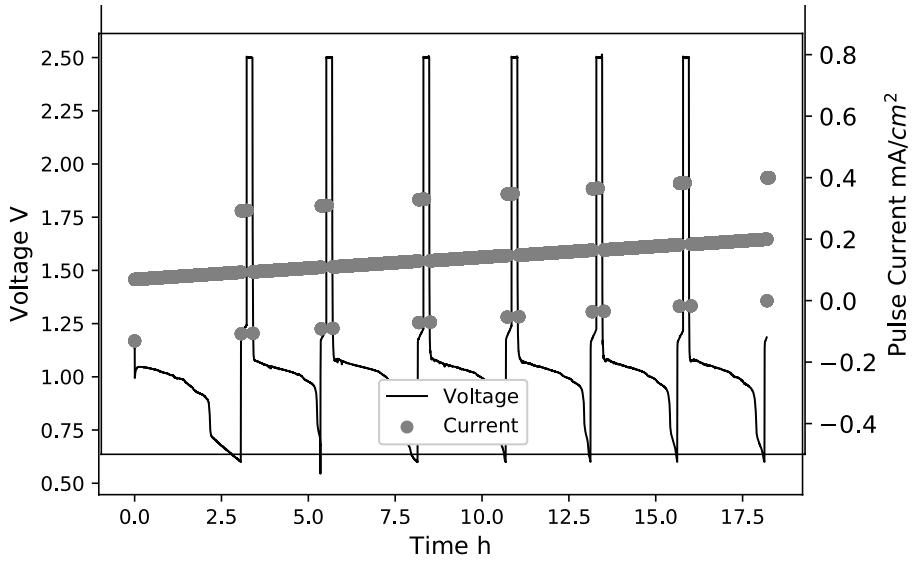

Figure 13. Pulse charge(10min) and slow discharge battery cycling data

The discharge current is 0.2mA/cm^2 and the charging current is 0.4mA/cm^2 accumulatively the battery has discharged over 3.5mAh/cm^2 doubled the best performing single battery using primary discharge test under the same discharge rate. During the charging cycle only 0.8mAh/cm^2 of charge is passed by the cell. Assume the charging efficiency is 100%, most of the charge during discharge process is not from the charging cycle. As a result, the high current charging cycle functions like a recovering cycle which reactivate the anode/electrolyte surface. In the previous study due to the nature of the particle-based anode and gel electrolyte, the utilization of zinc after primary discharge is 37%

3.5 Summary

Deep eutectic solvent is chosen as the active component in the solid-state electrolyte for zinc air battery. The flexible zinc air battery is prepared by printing each layer directly on top of the other one. Printing method includes screen printing, stencil printing and 3d printing. The advantage of printing everything sequentially is the simplicity and scalability of the processes. Our DES electrolyte contains urea, choline chloride and ZnO together with crosslinked PVA as the gel skeleton. These chemicals are considered biologically safe for human body since both urea and choline chloride are formed during normal metabolic processes of human body.[28,51] PVA and ZnO are also widely used on human body such as sunscreen and drug capsule. Compared with ionic liquid electrolyte and alkaline electrolyte, DES electrolyte is much more suitable for on body wearable applications.

The DES solid state electrolyte exhibits great ionic conductivity 1.2mS/cm at room temperature. The high ZnO solubility enables a higher discharge rate up to 0.4mA/cm^2 and adds rechargeability to the cells with more than 1.2mAh/cm^2. The cell is also integrated with roll to roll flexographic printing-based anode which mass producible and has smoother surface suitable for subsequent printing process.

Chapter 4: Printed DES Cell Optimization

4.1 Motivation

Previous work showed promising results and demonstrated fully printed ZAB cell structures and process flows based on ionic liquid and DES solvent electrolytes. The process is scalable and facile, however, the resulting devices suffer from several problems. Because the air cathode needs to be in contact with the air. Therefore, the obvious cell layer sequence is to deposit carbon on top of the electrolyte layer. The problem presented by printing carbon last is the extra heat treatment required to process the catalyst layer. During these two heat treatments the Zinc is in direct contact with the electrolyte which results in accelerated zinc corrosion. Therefore, we demonstrated a photo-crosslink process for the electrolyte layer which requires no heat treatment for the formation of a physically robust, stable electrolyte layer that allows for subsequent cell layer printing. Not only this process reduces the corrosion of zinc electrolyte but also it does not involve solvent evaporation which suffers significantly less from volumetric shrinkage. Therefore, this process also reduces the formation of pinholes and dewetting spots.

The particle-based anode has the problem of high porosity and high contact angle with the electrolyte. To have an electrically continuous conductive structure significant amount of conductive additive should be added. In previous experiments at least 8%wt is required to have good conductivity. Higher loading of carbon is beneficial for the high porosity and hydrophobicity of the anode. These two factors make the deposition of electrolyte difficult. On the other hand, the particles having size between 20-40um defines the minimum thickness of the electrode and to a degree the roughness of the

surface. It is difficult to control the thickness of anode due to this reason. Based on the reasons above, we propose electroplating the Zn instead. The pattern of the Zn layer is guided by printed conductive silver seed layer.

4.2 Device Architecture

The battery cell under development in this portion of the work has identical structure as the cells described in chapter 3. However, the way each layer was prepared differently. The lateral pattern of the anode layer is defined by the Ag current conductor using roll-to-roll flexographic printing method. Flexographic printing utilize engraved structures to define the pattern and transfer ink from an anilox ink metering roller to the printing substrate by physical contacting the substrate. It is particularly promising for this application because it is additive and compatible with roll-to-roll processes. Therefore it has the advantages of high-speed, high resolution, high throughput and scalability[52,53]. As shown in Figure 14 the flexographic plate structure is designed to have multiple pads and interdigitated electrodes which patterns the shape of latter pattern.

Electroplating was chosen as the process method for depositing the zinc layer. The main advantage is that electroplating has a better control of the film thickness. Since pure zinc is plated onto silver patterns, no binder or conductive additives are required for the process which further simplify the parameters. Without hydrophobic carbon content the wetting property of zinc layer can be largely improved.

The electrolyte layer is quite adaptable in terms of the methods can be used for deposition. This is because the electrolyte precursor does not contain solid

suspensions and is compatible with multiple additives for wetting and rheology tunning. The 3d printing is the method that was chosen for this layer. The reason is that it has the best control of the wet film thickness among other printing methods like screen printing, flexographic printing, and ink jet printing. 3D printing is also suitable for fast prototype preparation since it does not require masks, screens, or flex pads.

The final layer is the carbon-based cathode layer. Polyimide masks were used as stencils for stencil printing process of the carbon-based ink. The carbon ink contains multiwall carbon nanotubes, graphene-based catalyst, and a polymer binder such as polyvinylpyrrolidone. Carbon materials and especially carbon nanotubes are difficult to be formulated into consistent inks for printing processes. Obtaining stable printable CNT dispersion is a challenging undertaking in it's own right[42,54]. Ideal formulations includes a minimum amount of polymer binders to minimize the problem that polymer passivating the catalyst surface. Therefore, I decided to use the most robust way to deposit the carbon ink which is stencil printing. We can potentially control the wet film thickness with that of the stencil.

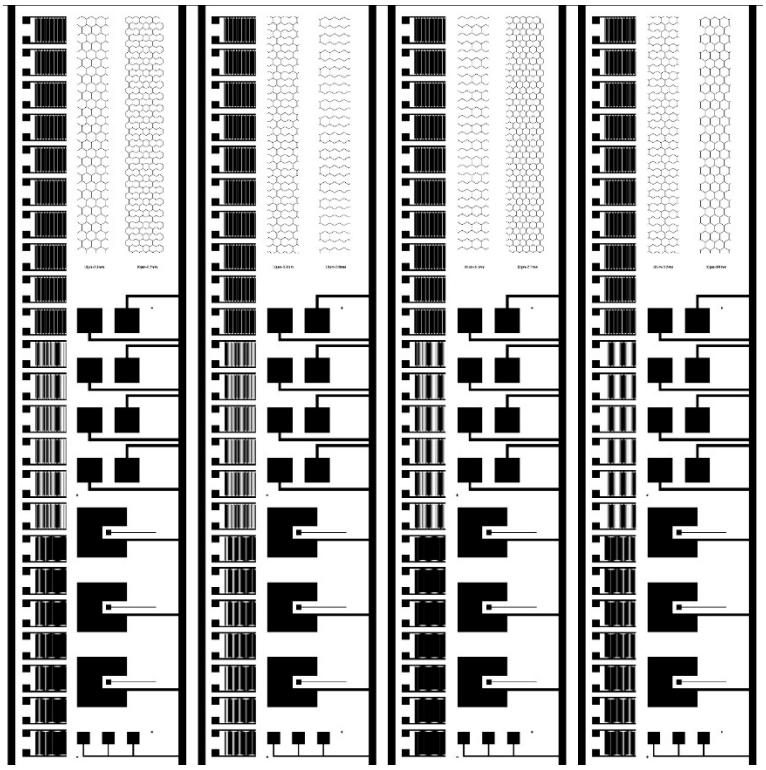

Figure 14. Bottom silver electrode pattern used for the flexographic printing plate.

4.3 Fabrication Method

Thermal Cured Solid Electrolyte: 3g of PVA (Polyvinyl Alcohol M.W 146,000~186,000, 99% hydrolyzed, Sigma Aldrich) was dissolved in 30ml DI water at 85 Celsius. Urea and choline chloride are mixed at molar ration 2:1 at 80Co. 1g of the DES mixture and 5g of the PVA solution was them homogenized in a planetary mixture at 1800rpm for 15min. Glutaraldehyde 3% (w/w) is the added to the mixture. The resulted DES/polymer ink was then coated on top of the zinc layer. The solid ionic polymer gel films were 20-30 μm in thickness. The Carbon layer is the same as our previous work.

Flexible Zinc Electrode Preparation: First the silver pattern is printed on polyimide substrates by flexography using FOM roll-to-roll system. One example of the silver pattern is shown in Figure 14. The patterns on each band are connected buy silver bus wires. The resulted silver pattern is then submerged in electroplating bath and plated at 12mA/cm^2 for 15min. The sample is then rinsed with copious amount of DI water. It is then dried for 20 minutes at 80 Celsius. The final film thickness of the printed Zn composite electrode was 12 μm.

Photo Crosslinked Solid Electrolyte: Urea and choline chloride are mixed at 80C^o for 4 hours. 5%(w/w) ZnO is then added to the solution slowly and stirred until the solution is clear with no visible ZnO particles. Various amount of acrylic acid is then added to the mixture after the DES mixture is cooled to room temperature. Finally 4-(2-hydroxyethoxy)phenyl-(2-hydroxy-2-propyl)ketone 0.5%(w/w), fumed silica particles 5%(w/w) and crosslinker poly(ethylene glycol) divinyl ether (PEGDE(Mn ≈

250g/mol)1%(w/w) are added to the ink before the coating process. The ink was then coated via doctor blade coating or extrusion based 3d printing on top of the zinc electrode. The sample is then exposed to UV light at power 3W/cm^2 for 10min.

A typical fabrication of the electrolyte is follows: First process of the deep eutectic solvent(DES) was prepared by mixing choline chloride and urea powders under the mole ratio of 1:2, then the mixture was heated(80 ℃) and stirred(800 rpm) on a hotplate for 2 h until completely dissolved. Next, 0.091 g zinc oxide was added to a 20 mL vial, followed by adding3.125 g prepared DES. After that, the vial was put into Thinky mixer for 5 min under the speed of 1800 rpm. When the zinc oxide was fully dissolved, 38 mg photoinitiator was added to the hybrid and mingled for 5 min. The next step was to add 0.368 g hydrophilic silica into the vial for the purpose of increasing the mixture viscosity. At this stage, the vial was mixed for 10 min. In the end, acrylic acid(0.5 mL), ethanol(0.5mL) and crosslinker(0.5 mL) were dropped into the container respectively. Again, thecompound was under mixed for 5 min. For the second part, the prepared solution was exposed to a UV lamp(350 W) for 10 min to form solid gels.

As shown in figure 12 after preparing the inks for each layer, each component was deposited on top of each other sequentially. After the deposition of Ag, Zn and CNT layer there was a brief baking process to remove excessive amount of solvent in the system.

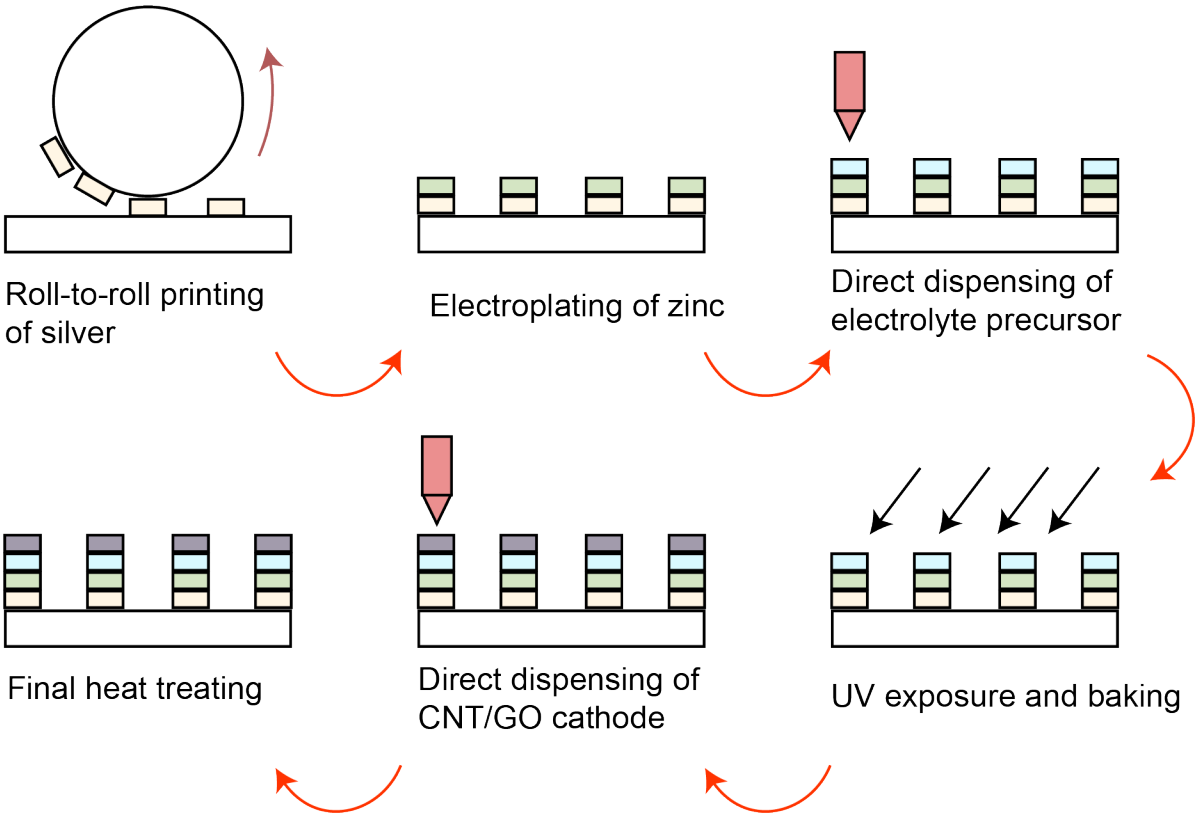

Figure 15. Improved processes for DES based ZAB

4.4 Characterization and Results

Figure 16 shows the micrograph of crosslinked electrolyte. The image was taken using laser microscope. The laser microscope does not require high vacuum which is sensitive to the fume created by the DES evaporation. The PAA forms little tunnels infiltrated by DES. Figure 17 shows the cross section of the discharged battery.The components from the left to the right are cathode, electrolyte, Zinc, and substrate. Since the thickness of the Ag is only 200nm, it is not noticeable in the micrograph. After long period of time discharging most of the zinc layer is consumed as well.

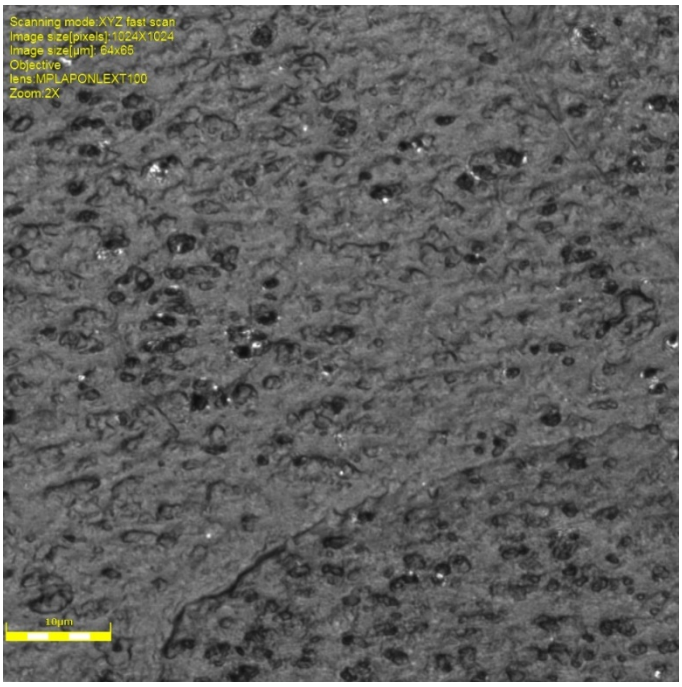

Figure 16. Laser microscopy image of DES electrolyte layer after UV exposure.

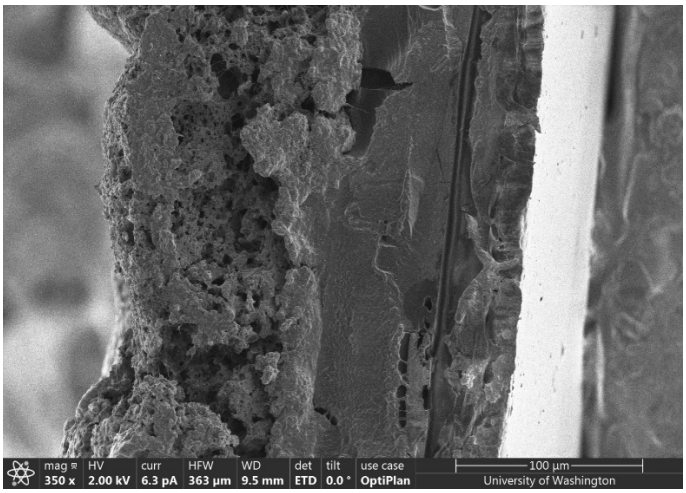

Figure 17. Cross sectional SEM image of the discharged battery

The electroplated zinc electrode morphology is dramatically different from the zinc powder-based electrode. The density of the electrode almost doubled. The zinc mass loading for a 12um electroplated is equivalent as a 20um zinc powder-based anode. The contact angle of electrolyte precursor on the anode also decreases from 94^{o} to 73^{o}. Having low contact angle and high density means our initial target of having electroplated zinc is achieved. As shown in Figure 19 the Ag seed layer is composed of nanoparticles. The print we are using has an average thickness of 200nm. Because its low thickness the film has large amount of void zones. The defects on the seed layer did not lead to detrimental impact on the zinc film structure.

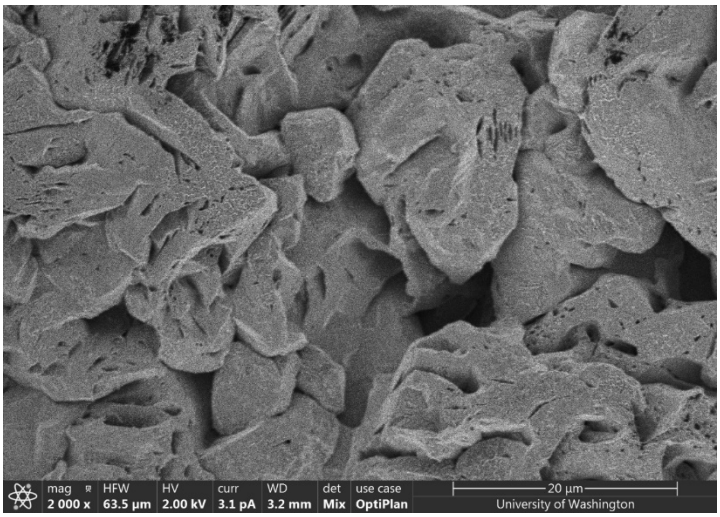

Figure 18. SEM image of the electroplated Zinc with room temperature and low current.

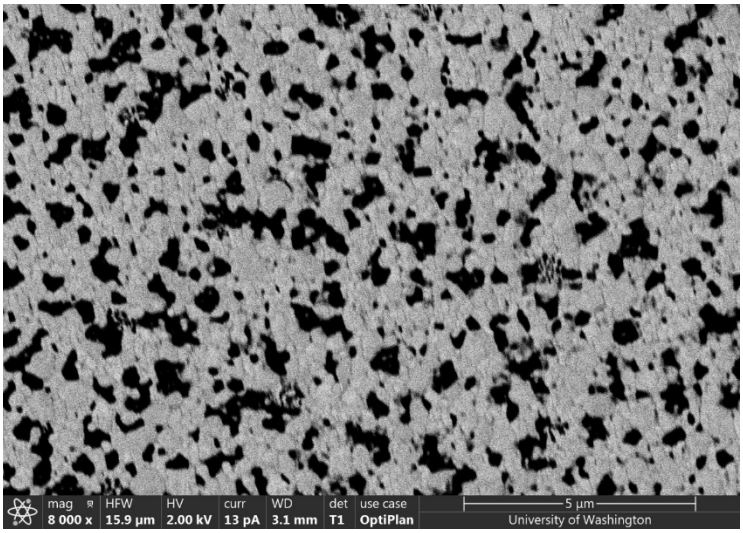

Figure 19. SEM image of the as deposited Ag layer

The process of UV initiated crosslinking is rapid. After 10min of exposure to the UV source the PAA electrolyte precursor converted to a solid-state electrolyte as shown in figure 20.

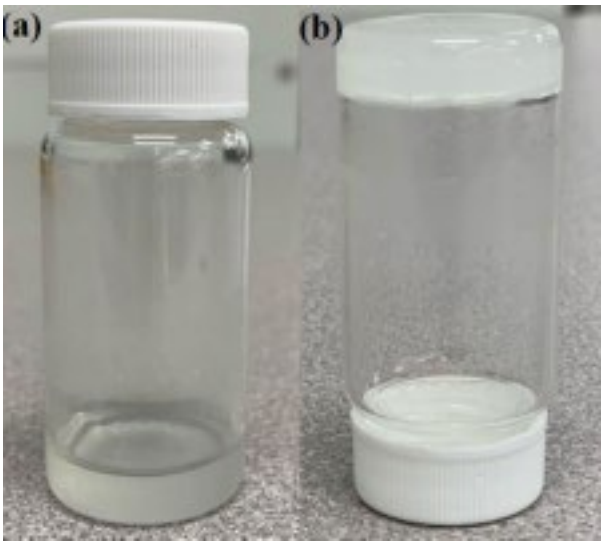

Figure 20. PAA electrolyte solution(a) and polymerized PAA electrolyte gel(b)

The resulted DES gel electrolyte was obtained carefully and measured between two stainless steel electrodes. Electrochemical impedance spectroscopy was measured with a Maccor battery tester and a temperature chamber. These measurements were implemented with cuboid samples (18*9*3.5 mm^3) of 2%ZnO-DES-SiO2-PAA gel from10 ℃to 90 ℃. The frequency of these experiments ranged from 10^5 to 1 Hz with an amplitude of 10mV. Figure 22 is the Nyquist plot based on the impedance spectroscopy data at room temperature. The data shows very small capacitance which indicates that the electrolyte does not have multiple grains which contributes to grain to grain capacitance. Since we are using polished stainless steel the electrode-electrolyte capacitance is also minimized. In this case the series resistance is taken as the real impedance when the imaginary part is zero. Knowing the dimensions of the electrolyte we can calculate the conductivity of electrolyte using the equation.

$$\kappa = \frac{L}{RA}$$

Where κ is the conductivity, L is the thickness, A is the area and R is the series resistance of the electrolyte.

As shown in Figure 21 the conductivity of electrolyte was measured in a temperature range between 10℃ to 80℃. The resulted data can be fitted into Arrhenius relationship with a R^2 close to 1:

$$ln\sigma = \ln \sigma_0 - \frac{E_a}{KT}$$

The activation energy is calculated to be 46.9kJ mol^{-1}. This value is approximately one order or magnitude larger than that of liquid choline chloride based DES mainly due to the fact that only 50%wt of the solid state electrolyte is actively conducting ions and the other half of the electrolyte is for holding the gel 3D structure which increases the difficulty to activate the ions. Despite the high activation energy the conductivity of the DES gel electrolyte is 1.01mS cm^{-1}. This number is consistent with the numbers measured in the literatures.[55,56]

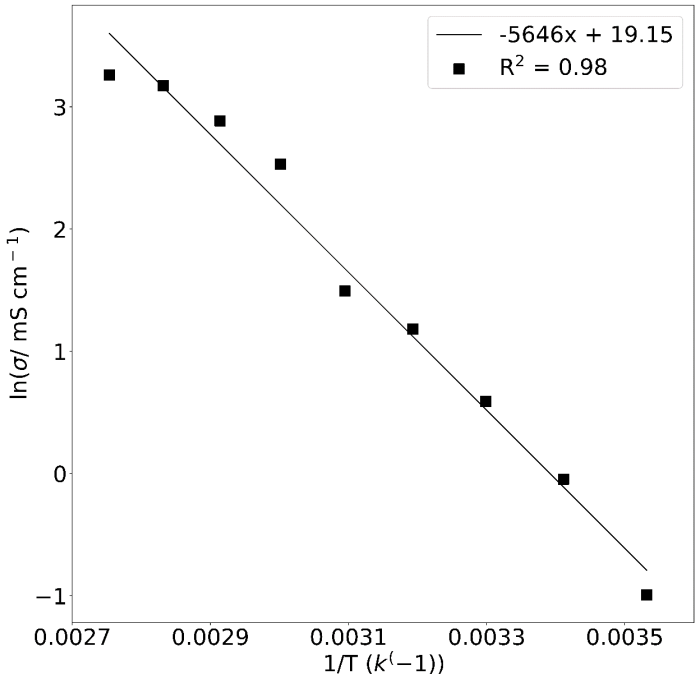

Figure 21. Electrolyte conductivity measurement over wide temperature span.

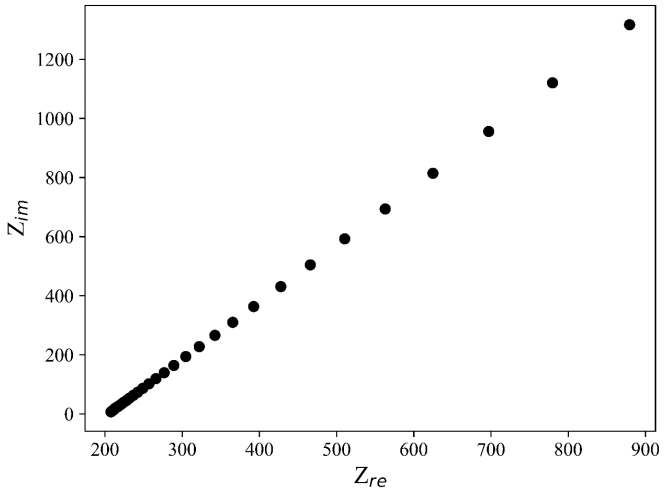

Figure 22.Nyquist plot of Electrolyte conductivity measurement at room temperature.

Frequency sweep experiment was implemented with conical plate (50 mm) mode in Modular Compact Rheometer—Anton Paar, under isothermal condition (25 ℃) at anormal force of 1N. The shear rate of this experiment ranged from0.01s^{-1} to 100s^{-1}. The gap between two conical plates were kept constant at 0.1 mm.

The electrolyte without SiO_2 additive behaves identical to a Newtonian fluid the average viscosity is 183.4mPa·s. This viscosity is not suitable for screen printing or 3D printing because low viscosity ink will result in ink over spread after the patterning process. Ideally for 3D printing we need the ink to have low viscosity at high shear rate because this is when we are pushing the ink out of the nozzle. High viscosity at low shear rate is also desirable because ink spread out after dispensing process is problematic.[57] As shown in Figure 23 after adding fumed silica particles to the ink, a shear thinning fluid is obtained and the viscosity is 1 order of magnitude higher that the control sample.

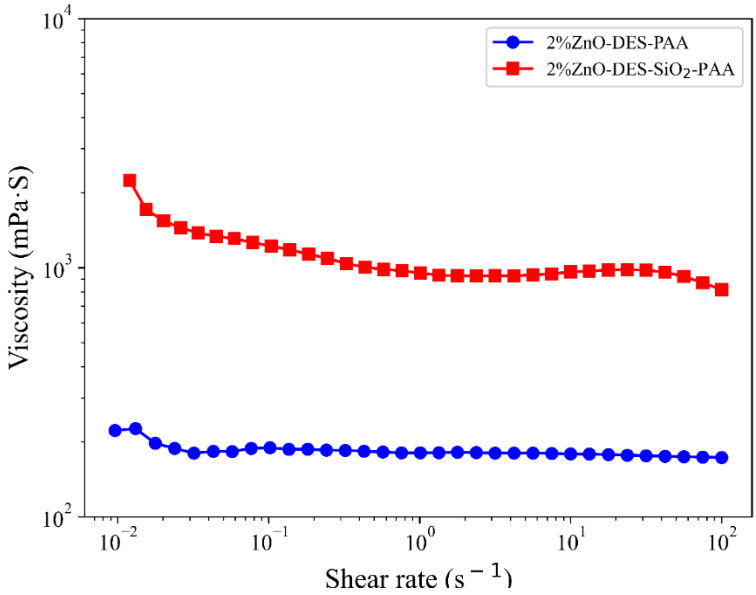

Figure 23. Rheology data of DES-PAA Precursor

It is important that the thermal stability window of the electrolyte. The other parts of the device are made of metal or carbon which can operate at temperatures higher than 300℃. So, the thermal stability of the electrolyte determines the maximum temperature that the battery theoretically can operate. Based on the data shown in Figure 21 and Figure 22 the DES-PAA electrolyte is stable up to 150℃ despite the water loses peak of the derivative data at 100℃. Increasing the heating rate from 5℃/min to 15℃/min during TGA sweep shift onsite temperature slightly but the obtained data is consistent as well.

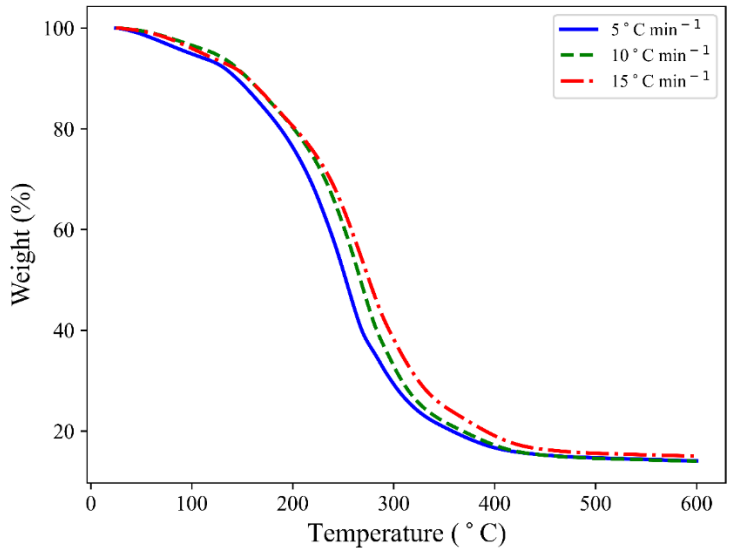

Figure 24. TGA data of DES-PAA Electrolyte

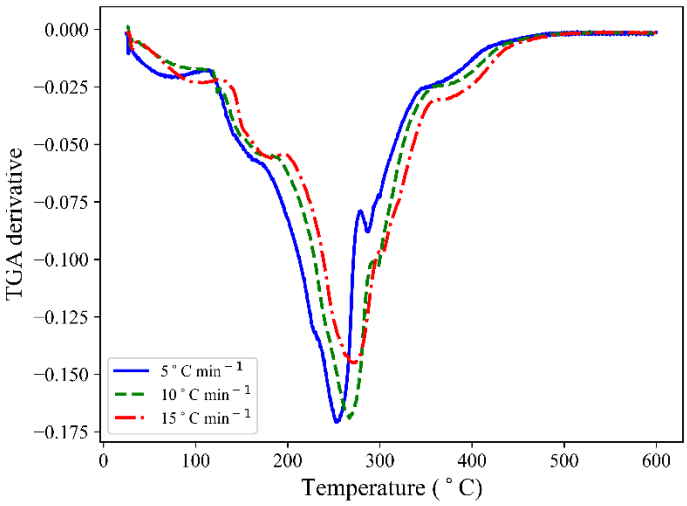

Figure 25. TGA derivative vs Temperature

With all the changes on the processes and materials, the final devices' performance is tested. As shown in Figure 26 compared with the battery using ionic liquid electrolyte, the DES based cells have a higher capacity at all current density. Especially at very low

current situation when the IL suffers from CO_2 poisoning the DES cells show extraordinary capacity. The primary discharge lasts over 50 hours and no DES degradation problem was observed.

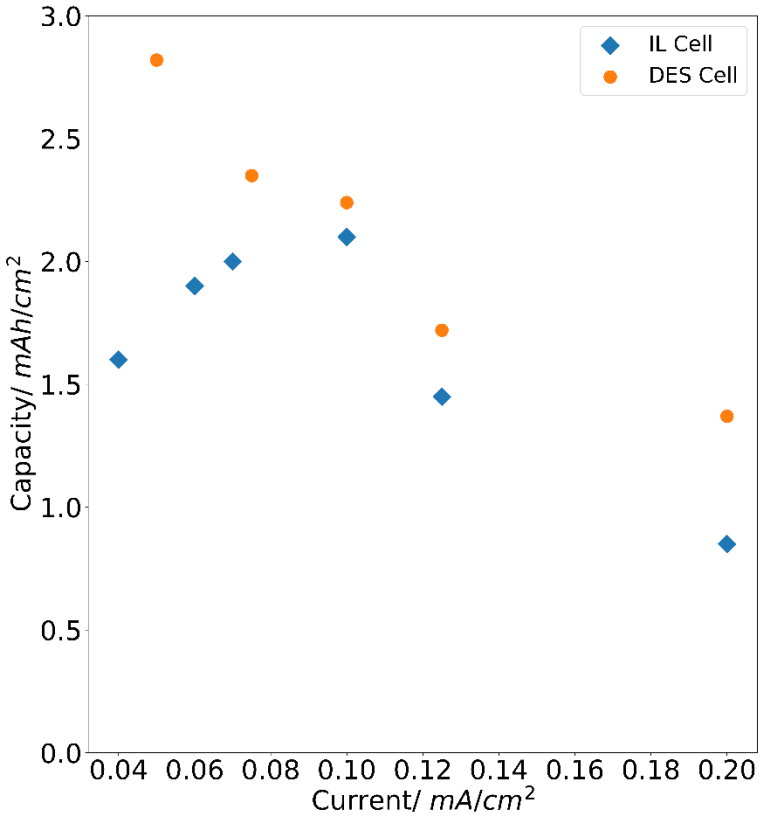

Figure 26. Discharge capacity comparison between DES and RTIL cells

Figures 27 and 28 are the discharge profiles of printed batteries containing ionic liquid and DES electrolyte. The current density is 0.2mA/cm^2. As shown in the figures when using DES as the electrolyte not only the capacity is increased by 89%, the working potential is also increased to 0.8V from below 0.6V.

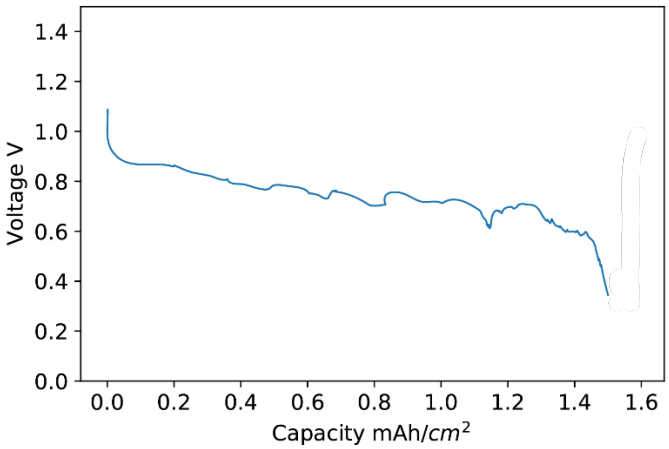

Figure 27. DES cell primary discharge profile(0.2mA/cm^2)

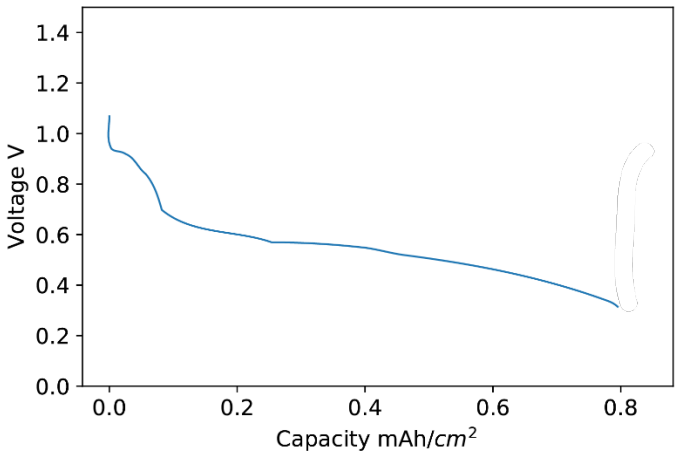

Figure 28. RTIL cell primary discharge profile(0.2mA/cm^2)

As shown in Figure 29 the battery can operate at lower temperatures. As discussed earlier the ion transport activation energy is large for this electrolyte. As a result there is a substantial decrease of working potential from 0.8V to 0.4V. For the low temperature measurement at the end of the discharge an open circuit voltage is recorded. The

sample measured at 10 °C recovered 98% of it's open circuit voltage after the discharge which also indicates that concentration polarization contributes most to the voltage lost.

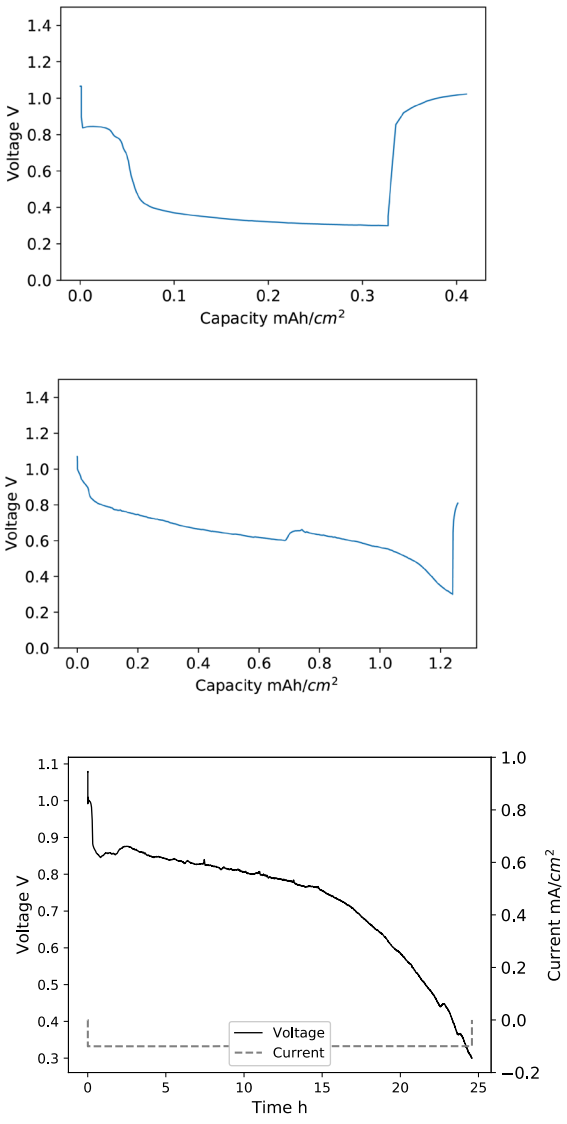

Figure 29. Primary discharge profile of DES cell at 10°C(top), 20 °C(middle) and 30 °C(bottom)

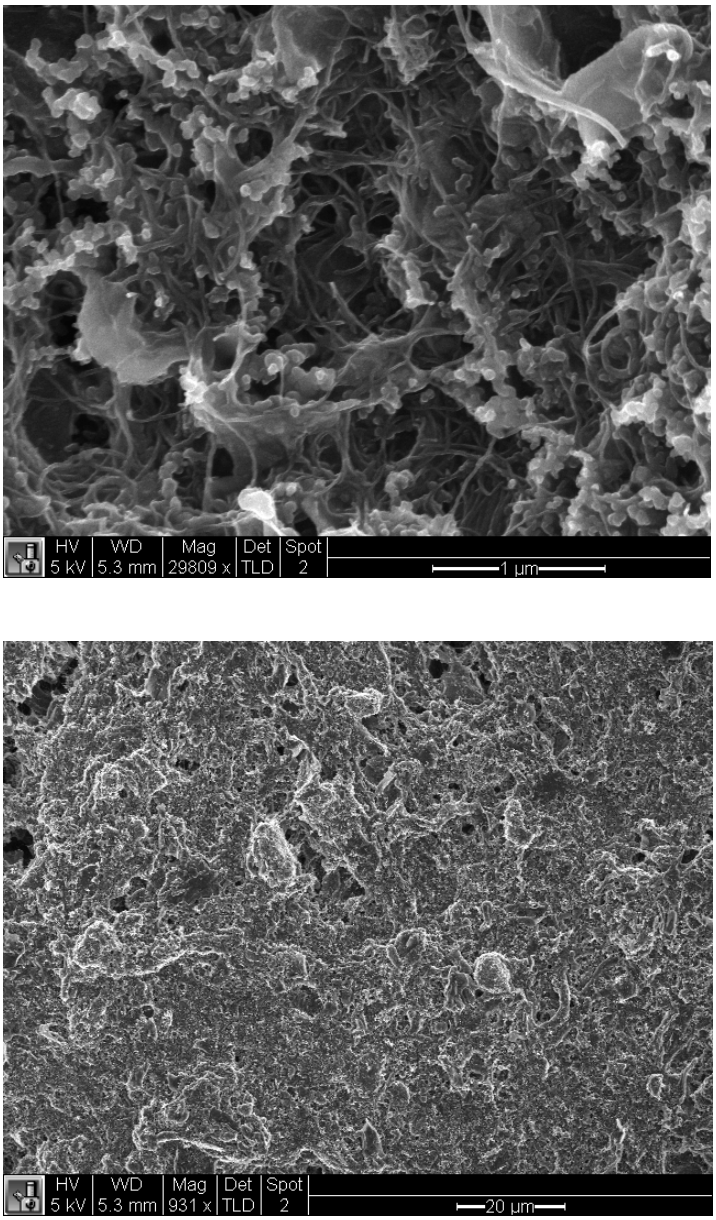

Figure 30. SEM images of carbon electrode with PVP binder

To optimize the power density and capacity the cathode should have as high surface area as possible. This makes the choice of additives to the cathode ink very limited. In the previous study no polymeric binder was used on cathode. Figure 30 shows the microstructure of the cathode with polymer binder. In this case the polymer is PVP. The

high magnification image clearly shows that the binder holds the carbon materials and keep the structure homogeneous and stable.

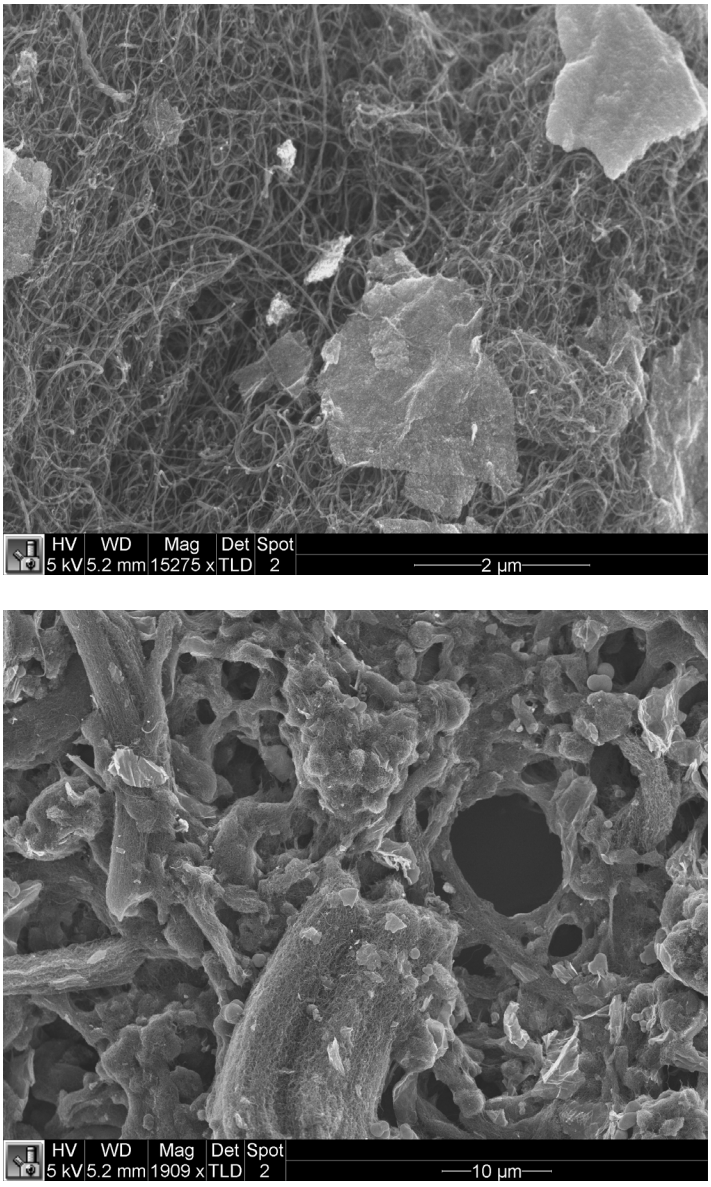

Figure 31. SEM images of carbon electrode without PVP binder

On the other hand in Figure 31. Cathode without polymeric binders is shown. Since there is no polymer binder, the number of pores is much higher and the force that holds

the carbon together is not from the binder. In this case is the inter molecular force between carbons.

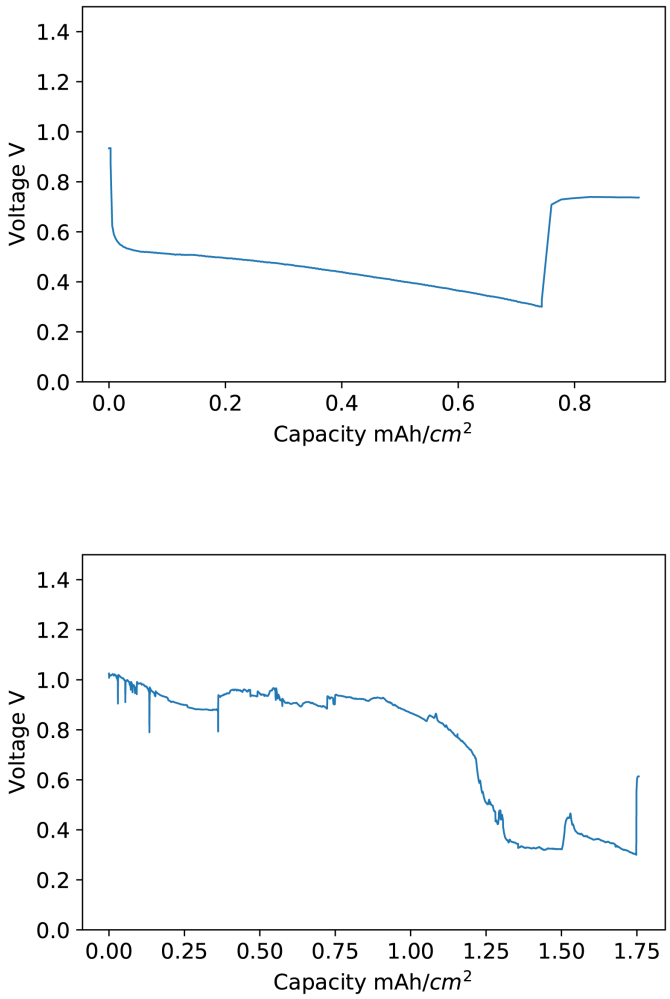

Figure 32. Discharge profile comparison between sample containing PVP binder in cathode(top) and sample without PVP binder in cathode(bottom)

Figure 32. shows the discharge profile from the cathodes with and without PVP binder. There are 3 main differences between the samples. The sample contains no PVP has a much higher capacity. The sample with PVP exibits a mch lower working potential. The reason is that the PVP covered the active reaction site which slows down the reaction. The reaction rate of ORR

is already the bottleneck of the cell. As a result the drop of working potential is significant. The last difference between the to sample is the level of noise. Although the sample with binder does not perform as well as the one without, it has a much lower level of noise. As explained earlier the binder improves the mechanical stability of the cathode. Since the noise completely goes a way by adding binder to the cathode, it can be conclude that the high level of noise in previous sample data are coming from the cathode instabiliy.

4.5 Summary

In this chapter the zinc air battery using DES electrolyte has been optimized for the first time in a ZAB. New processes are investigated for each individual layers. a thinner bottom current collector and electroplating template using high speed roll-to-roll method, the total thickness of the battery reduces which increases the charge density. A photo initiated crosslinking method is used to obtain DES/PAA electrolyte gel. This process removes the heat treatment involved in the previous chemical crosslinking method. One less heat treatment will significantly reduce the corrosion of the zinc electrode. Since it does not involve solvent evaporation the volumetric change of the film is minimized as well.

The impact of adding binders to the cathode was also studied. As a conclusion, mechanical instability is the main contributor to the voltage noise during discharge. Adding polymeric binders will help stabilize the electrode. However, the polymer also blocks the pores and catalyst active sites which slows down the critical ORR.

Chapter 5: Conclusions

In summary, a completely printed thin film zinc-air battery has been demonstrated for the first time via a layer-by-layer monolithic additive process without electrolyte filling after cell fabrication. This monolithic process was enabled by the high thermal stability and low vapor pressure of the sold ionic liquid electrolyte films. These printed thin film batteries exhibited high volumetric capacities of 200 AhL^{-1} as compared to commercially-available thin film lithium polymer batteries and represents, as far as the authors are aware, the highest areal capacity(2.0mAh cm^{-2}) for any cells with thicknesses below 160 μm.[1] For batteries below 500 μm in total thickness, an aerial capacity of 2.4mAh cm^{-2} is higher than that of other flexible batteries.[2,3] The ionic liquid gel-based electrolyte is stable throughout the fabrication process which includes, cumulatively, 90 minutes of heat treatment at 80 C^{o}. Our new DES electrolyte and anode fabrication technique allow us to further reduce the overall thickness and make our battery electrolyte biodegradable. The screen printing and stencil printing tools employed for open-air processing in this study are widely available and scalable to high production throughputs. This additive printing approach could readily be translated to large scale, low cost, and low carbon footprint production of truly thin film batteries to power next generation, low toxicity, sustainable medical devices, wearable electronics and IoT devices. As discussed in the introduction there are several criteria for a good flexible battery to power IoT devices. The table below is a summary of the battery characteristics. After the process improvement and material selection the cells meet most of the criteria.

Capacity for 1 day usage	Good
Battery pulse discharge capability	Good
Human body safe materials	Anode and electrolyte are safe
Low modulus and thickness	Good
All solid-state Electrolyte	Good
Low vapor pressure electrolyte	Good
Thermal stable electrolyte up to 120C	Good

Table 1. Battery characteristic summary

These processing methods, cell designs and materials have a very optimistic potential. We demonstrated that with optimization of each individual components the capacity and reliability of the battery can be significantly improved. As far as the author aware, there is no literatures studying the printing process of zinc air batteries using DES or RTIL as electrolyte. This paper shows the possibility of printing a zinc air battery using a layer-by-layer strategy. It has also been shown that for ultrathin wearable applications DES or RTILs are very promising electrolyte candidates. The impact of each component, process and additives was studied. There is little doubt that the capacity and power density will keep increasing as we make each individual layer better.

Bibliography

1. MacKenzie, J. D. & Ho, C. Perspectives on Energy Storage for Flexible Electronic Systems. *Proc. IEEE* **103**, 535–553 (2015).
2. Liu, Q., Chang, Z., Li, Z. & Zhang, X. Flexible Metal–Air Batteries: Progress, Challenges, and Perspectives. *Small Methods* **2**, 1700231 (2018).
3. Liu, T. *et al.* Ultrathin, Lightweight, and Wearable Li-O2 Battery with High Robustness and Gravimetric/Volumetric Energy Density. *Small* **13**, 1602952 (2017).
4. Mukhopadhyay, S. C. Wearable Sensors for Human Activity Monitoring: A Review. *IEEE Sens. J.* **15**, 1321–1330 (2015).
5. Honda, W., Harada, S., Arie, T., Akita, S. & Takei, K. Wearable, Human-Interactive, Health-Monitoring, Wireless Devices Fabricated by Macroscale Printing Techniques. *Adv. Funct. Mater.* **24**, 3299–3304 (2014).
6. Savagatrup, S. *et al.* Viability of stretchable poly(3-heptylthiophene) (P3HpT) for organic solar cells and field-effect transistors. *Synth. Met.* **203**, 208–214 (2015).
7. Teizer, J. Wearable, wireless identification sensing platform: Self-Monitoring Alert and Reporting Technology for Hazard Avoidance and Training (SmartHat). *J. Inf. Technol. Constr. ITcon* **20**, 295–312 (2015).
8. Maier, D. *et al.* Toward Continuous Monitoring of Breath Biochemistry: A Paper-Based Wearable Sensor for Real-Time Hydrogen Peroxide Measurement in Simulated Breath. *ACS Sens.* **4**, 2945–2951 (2019).
9. Seneviratne, S. *et al.* A Survey of Wearable Devices and Challenges. *IEEE Commun. Surv. Tutor.* **19**, 2573–2620 (2017).

10. Dementyev, A., Hodges, S., Taylor, S. & Smith, J. Power consumption analysis of Bluetooth Low Energy, ZigBee and ANT sensor nodes in a cyclic sleep scenario. in *2013 IEEE International Wireless Symposium (IWS)* 1–4 (2013). doi:10.1109/IEEE-IWS.2013.6616827.
11. Gelman, D., Shvartsev, B. & Ein-Eli, Y. Aluminum–air battery based on an ionic liquid electrolyte. *J. Mater. Chem. A* **2**, 20237–20242 (2014).
12. Fu, J. *et al.* Electrically Rechargeable Zinc–Air Batteries: Progress, Challenges, and Perspectives. *Adv. Mater.* **29**, n/a-n/a (2017).
13. Strauss, E., Menkin, S. & Golodnitsky, D. Polymer Electrolytes for Printed Batteries. in *Printed Batteries* 80–111 (John Wiley & Sons, Ltd, 2018). doi:10.1002/9781119287902.ch4.
14. Qu, H., Hou, J., Tang, Y., Semenikhin, O. & Skorobogatiy, M. Thin flexible lithium-ion battery featuring graphite paper based current collectors with enhanced conductivity. *Can. J. Chem.* **95**, 169–173 (2016).
15. Gaikwad, A. M. *et al.* A High Areal Capacity Flexible Lithium-Ion Battery with a Strain-Compliant Design. *Adv. Energy Mater.* **5**, n/a-n/a (2015).
16. Li, Y. *et al.* Advanced zinc-air batteries based on high-performance hybrid electrocatalysts. *Nat. Commun.* **4**, 1805 (2013).
17. Zhang, J. *et al.* Laminated Cross-Linked Nanocellulose/Graphene Oxide Electrolyte for Flexible Rechargeable Zinc–Air Batteries. *Adv. Energy Mater.* **6**, n/a-n/a (2016).
18. Chen, X. *et al.* Ultrathin Co3O4 Layers with Large Contact Area on Carbon Fibers as High-Performance Electrode for Flexible Zinc–Air Battery Integrated with Flexible Display. *Adv. Energy Mater.* n/a-n/a doi:10.1002/aenm.201700779.
19. Fu, J. *et al.* Flexible High-Energy Polymer-Electrolyte-Based Rechargeable Zinc–Air Batteries. *Adv. Mater.* **27**, 5617–5622 (2015).

20. Caramia, V. & Bozzini, B. Materials science aspects of zinc–air batteries: a review. *Mater. Renew. Sustain. Energy* **3**, 28 (2014).
21. Suren, S. & Kheawhom, S. Development of a High Energy Density Flexible Zinc-Air Battery. *J. Electrochem. Soc.* **163**, A846–A850 (2016).
22. R. Mainar, A. *et al.* Alkaline aqueous electrolytes for secondary zinc–air batteries: an overview. *Int. J. Energy Res.* **40**, 1032–1049 (2016).
23. Wang, Z., Meng, X., Wu, Z. & Mitra, S. Development of flexible zinc–air battery with nanocomposite electrodes and a novel separator. *J. Energy Chem.* **26**, 129–138 (2017).
24. Hilder, M., Winther-Jensen, B. & Clark, N. B. Paper-based, printed zinc–air battery. *J. Power Sources* **194**, 1135–1141 (2009).
25. Wu, H. *et al.* Transfer Printing of Metallic Microstructures on Adhesion-Promoting Hydrogel Substrates. *Adv. Mater.* **27**, 3398–3404 (2015).
26. Armand, M., Endres, F., MacFarlane, D. R., Ohno, H. & Scrosati, B. Ionic-liquid materials for the electrochemical challenges of the future. *Nat. Mater.* **8**, 621–629 (2009).
27. SHI Chaojun,HO Christine C.,MACKENZIE J. Devin. Ionic Liquid Gel for Electrolyte, Method of and Ink for Making the Same, and Printed Batteries Including Such Ionic Liquid Gels and/or Electrolytes. (2017).
28. Hirsch, M. J., Growdon, J. H. & Wurtman, R. J. Relations between dietary choline or lecithin intake, serum choline levels, and various metabolic indices. *Metabolism* **27**, 953–960 (1978).
29. Marvel, J. A., Carrick, C. W., Roberts, R. E. & Hauge, S. M. The Supplementary Value of Choline and Methionine in a Corn and Soybean Oil Meal Chick Ration1,2. *Poult. Sci.* **23**, 294–297 (1944).
30. Radošević, K. *et al.* Evaluation of toxicity and biodegradability of choline chloride based deep eutectic solvents. *Ecotoxicol. Environ. Saf.* **112**, 46–53 (2015).

31. Song, Z. *et al.* Carbon hydrangeas with typical ionic liquid matched pores for advanced supercapacitors. *Carbon* **168**, 499–507 (2020).
32. Yadav, N., Yadav, N. & Hashmi, S. A. Ionic liquid incorporated, redox-active blend polymer electrolyte for high energy density quasi-solid-state carbon supercapacitor. *J. Power Sources* **451**, 227771 (2020).
33. Xu, J. J., Ye, H. & Huang, J. Novel zinc ion conducting polymer gel electrolytes based on ionic liquids. *Electrochem. Commun.* **7**, 1309–1317 (2005).
34. Dueramae, I., Okhawilai, M., Kasemsiri, P., Uyama, H. & Kita, R. Properties enhancement of carboxymethyl cellulose with thermo-responsive polymer as solid polymer electrolyte for zinc ion battery. *Sci. Rep.* **10**, 12587 (2020).
35. Dou, Q. *et al.* "Water in salt/ionic liquid" electrolyte for 2.8 V aqueous lithium-ion capacitor. *Sci. Bull.* **65**, 1812–1822 (2020).
36. Zhu, Y. *et al.* A Composite Gel Polymer Electrolyte with High Performance Based on Poly(Vinylidene Fluoride) and Polyborate for Lithium Ion Batteries. *Adv. Energy Mater.* **4**, n/a-n/a (2014).
37. Wu, R. *et al.* Unveiling the intrinsic reaction between silicon-graphite composite anode and ionic liquid electrolyte in lithium-ion battery. *J. Power Sources* **473**, 228481 (2020).
38. Ogawa, T. *et al.* Coordination polymer glass from a protic ionic liquid: proton conductivity and mechanical properties as an electrolyte. *Chem. Sci.* **11**, 5175–5181 (2020).
39. Li, Y. *et al.* Modifying the Electrocatalyst–Ionomer Interface via Sulfonated Poly(ionic liquid) Block Copolymers to Enable High-Performance Polymer Electrolyte Fuel Cells. *ACS Energy Lett.* **5**, 1726–1731 (2020).
40. Sun, W. *et al.* A rechargeable zinc-air battery based on zinc peroxide chemistry. *Science* **371**, 46–51 (2021).

41. Liang, Y. *et al.* Covalent Hybrid of Spinel Manganese–Cobalt Oxide and Graphene as Advanced Oxygen Reduction Electrocatalysts. *J. Am. Chem. Soc.* **134**, 3517–3523 (2012).
42. Zhang, Q. *et al.* Fluffy carbon nanotubes produced by shearing vertically aligned carbon nanotube arrays. *Carbon* **47**, 538–541 (2009).
43. Pei, P., Wang, K. & Ma, Z. Technologies for extending zinc–air battery's cyclelife: A review. *Appl. Energy* **128**, 315–324 (2014).
44. Zhu, X., Wang, B. & Wang, H. Effects of [Bmim]OH on structure and conductive properties of alkaline PVA/[Bmim]OH membranes. *Polym. Bull.* **65**, 719–730 (2010).
45. Gaikwad, A. M., Whiting, G. L., Steingart, D. A. & Arias, A. C. Highly Flexible, Printed Alkaline Batteries Based on Mesh-Embedded Electrodes. *Adv. Mater.* **23**, 3251–3255 (2011).
46. Achieving Ultrahigh Energy Density and Long Durability in a Flexible Rechargeable Quasi-Solid-State Zn–MnO2 Battery - Zeng - 2017 - Advanced Materials - Wiley Online Library. https://onlinelibrary-wiley-com.offcampus.lib.washington.edu/doi/full/10.1002/adma.201700274.
47. Braam Kyle & Subramanian Vivek. A Stencil Printed, High Energy Density Silver Oxide Battery Using a Novel Photopolymerizable Poly(acrylic acid) Separator. *Adv. Mater.* **27**, 689–694 (2014).
48. MacFarlane, D. R. *et al.* Ionic liquids and their solid-state analogues as materials for energy generation and storage. *Nat. Rev. Mater.* **1**, 15005 (2016).
49. Kar, M., Simons, T. J., Forsyth, M. & MacFarlane, D. R. Ionic liquid electrolytes as a platform for rechargeable metal–air batteries: a perspective. *Phys. Chem. Chem. Phys.* **16**, 18658–18674 (2014).
50. Ingale, P., Sakthivel, M. & Drillet, J.-F. Test of Diethylmethylammonium Trifluoromethanesulfonate Ionic Liquid as Electrolyte in Electrically Rechargeable Zn/Air Battery. *J. Electrochem. Soc.* **164**, H5224–H5229 (2017).
51. Wrong, O. M. & Vince, A. Urea and ammonia metabolism in the human large intestine. *Proc. Nutr. Soc.* **43**, 77–86 (1984).

52. Huang, Q. & Zhu, Y. Gravure Printing of Water-based Silver Nanowire ink on Plastic Substrate for Flexible Electronics. *Sci. Rep.* **8**, 15167 (2018).

53. Secor, E. B. *et al.* Gravure Printing of Graphene for Large-area Flexible Electronics. *Adv. Mater.* **26**, 4533–4538 (2014).

54. Lawes, S., Riese, A., Sun, Q., Cheng, N. & Sun, X. Printing nanostructured carbon for energy storage and conversion applications. *Carbon* **92**, 150–176 (2015).

55. Harifi-Mood, A. R. & Buchner, R. Density, viscosity, and conductivity of choline chloride+ethylene glycol as a deep eutectic solvent and its binary mixtures with dimethyl sulfoxide. *J. Mol. Liq.* **225**, 689–695 (2017).

56. Millia, L. *et al.* Bio-inspired choline chloride-based deep eutectic solvents as electrolytes for lithium-ion batteries. *Solid State Ion.* **323**, 44–48 (2018).

57. Corker, A., C.-H. Ng, H., J. Poole, R. & García-Tuñón, E. 3D printing with 2D colloids: designing rheology protocols to predict 'printability' of soft-materials. *Soft Matter* **15**, 1444–1456 (2019).